The Role of C-X-C motif chemokine 12 in the crosstalk of brown adipocytes and microvascular endothelial cells

Doctoral thesis

to obtain a doctorate

from the Faculty of Medicine

of the University of Bonn

Max Retiet

from Saarbrücken, Germany

2025

Written with authorization of

the Faculty of Medicine of the University of Bonn

First reviewer: Prof. Dr. med. Alexander Pfeifer

Second reviewer: PD Dr. Philipp Lingohr

Day of oral examination: 10.03.2025

From the Institute for pharmacology and toxicology

To Katja, Luka, Inga, Malte & Andrej.

Table of Contents

List of Abbreviations

^{18}F-FDG PET-CT	^{18}Fluorodeoxyglucose positron-emission tomographic and computed tomographic
AC	Adenylate cyclase
Ackr3	Atypical chemokine receptor 3 gene
ACKR3	Atypical chemokine receptor 3
AIDS	Acquired immunodeficiency syndrome
ANOVA	Analysis of variance
ATP	adenosine triphosphate
BA	Brown Adipocyte
BAT	Brown Adipose Tissue
BMI	Body mass index
BMP7	Bone morphogenetic protein 7
BSA	Bovine serum albumin
C/EBPs	CCAAT/Enhancer-binding-proteins
$CaCl_2$	Calcium chloride
cAMP	3’-5’-cyclic adenosine monophosphate
CO_2	Carbon dioxide
CVDs	Cardiovascular diseases
Cxcl12	CXC motif chemokine ligand 12 gene
CXCL12	CXC motif chemokine ligand 12
Cxcr4	CXC motif chemokine receptor 4 gene
CXCR4	CXC motif chemokine receptor 4
Cxcr7	CXC motif chemokine receptor 7 gene
CXCR7	CXC motif chemokine receptor 7
ddH_2O	Double distilled water
DEPC	Diethyl pyrocarbonate
dH_2O	distilled Water

DMEM	Dulbecco modified eagle medium
DMSO	Dimethyl sulfoxide
EC	Endothelial Cells
ELISA	Enzyme-linked immunosorbent assay
Elovl3	Elongation of very long chain fatty acids 3
ERK1/2	Extracellular signal-regulated kinase ½
EtOH	Ethanol
Fabp4	Fatty acid binding protein 4
FBS	Fetal bovine serum
GDP	Guanosine diphosphate
GPCR	G protein-coupled receptor
GRK	G protein-coupled receptor kinase
GTP	Guanosine-triphosphate
HCl	Hydrochloride acid
HEPES	4-(2-hydroxyethyl)-1-piperazineethanesulfonic acid
Hif1α	Hypoxia inducible factor 1α gene
HIF1α	Hypoxia inducible factor 1α
Hif2α	Hypoxia inducible factor 2α gene
HIF2α	Hypoxia inducible factor 2α
HIV	Human immunodeficiency virus
Hprt	Hypoxanthine-guanine phosphoribosyl transferase gene
IBMX	3-isobutyl-1-methylxanthin
IP3	Inostiol-3-phosphate
JAK	Janus kinase
KCl	Potassium chloride
KH_2PO_4	Potassium dihydrogen phosphate
LESTR	Leukocyte-derived seven-transmembrane domain receptor

MAP kinase	Mitogen activated protein kinase
MEC	Microvascular endothelial cell
mRNA	Messenger ribonucleic acid
muMEC	Murine microvascular endothelial cell
Na_2HPO_4	Disodium hydrogen phosphate
Na_3VO_4	Sodium orthovanadate
NaCl	Sodium chloride
NaF	Sodium fluoride
NaOH	Sodium hydroxide
NE	Norepinephrine
NFκB	Nuclear factor kappa-light-chain enhancer of activated B-cells
NST	Non-shivering-thermogenesis
O_2	Oxygen
P/S	Penicillin/Streptomycin
PBGF	Pre-B cell growth factor
PBS	Phosphate buffered saline
PBS-T	Phosphate buffered saline 0.1% Tween®
PDE	Phosphodiesterase
PFA	Paraformaldehyde
PGC-1α	Peroxisome proliferator-activated receptor gamma coactivator 1-alpha
PKA	Protein kinase A
PLC	Phospholipase C
PPARγ	Peroxisome proliferator-activated receptor gamma
PRDM16	PRD1-BF1-RIZ1 domain containing 16
rpm	Revolutions per minute
RT	Room temperature
RT-qPCR	real-time quantitative polymerase chain reaction

SDF1	stromal-cell derived factor 1
SDS	Sodium dodecylsulfate
SEM	Standard error of the mean
SNS	Sympathetic nervous system
STAT	Signal transducer and activator of transcription
T3	Triiodthyronine
TAG	Triacylglycerol
Ucp1	Uncoupling protein-1 gene
UCP1	Uncoupling protein-1
WA	White adipocyte
WAT	White Adipose Tissue
WHIM-syndrome	Warts, hypogammaglobulinemia, infections, myelokathexis-syndrome

1. Introduction

1.1 Obesity

Since the 1980s the prevalence of obesity has been increasing worldwide (Afshin et al., 2017; Finucane et al., 2011; Roberto et al., 2015). Obesity is caused by an imbalance of energy intake and energy expenditure: energy-dense foods with high amount of sugar and fat are being consumed more often, while the overall physical activity and therefore energy expenditure is being reduced. The “Body Mass Index” (BMI) is a measure of body fat and can be used to classify overweight and obesity (weight-for-height index):

$$BMI = \frac{body\ weight\ (kg)}{body\ height\ (m)^2}\ .$$

Adults with a BMI greater than 25 are considered to be overweight; those who exceed a BMI of 30 are considered to be obese (WHO, 2021c).

To date, cardiovascular diseases (CVDs) such as coronary heart disease, cerebrovascular disease etc., are the number one cause of deaths in the world (WHO, 2021a). One major risk factor for CVDs is obesity. However, obesity does not only increase the risk for cardiovascular events, it is also a risk factor for type 2 diabetes, musculoskeletal disorders as well as certain forms of cancer and even psychiatric disorders (Ni Mhurchu et al., 2004; Simon et al., 2006; WHO, 2021b, 2021c). Additionally, it has been shown that overweight and obesity are associated with an increase in mortality (Prospective Studies Collaboration, 2009).

Key therapeutic strategies to tackle the obesity pandemic mainly focus on individual lifestyle changes. Patients who are trying to reduce their weight are advised to reduce their intake of high calorie foods and engage into physical activity on a regular basis (WHO, 2021c). Besides lifestyle changes, for some patients, bariatric surgery offers an additional effective way to treat obesity. Yet, one has to consider that the standard bariatric surgery procedures are irreversible and that peri- as well as postsurgical complications may occur (Benaiges et al., 2015; Kassir et al., 2016). From a pharmacological point of view, therapeutic options to treat obesity are fairly limited. In 2022 in Germany, orlistat (an inhibitor of gastric and pancreatic lipases) was the only drug recommended for treatment

of obesity (Deutsche Adipositas-Gesellschaft (DAG) e.V. et al., 2014). A Cochrane meta-analysis showed that the use of orlistat leads to significant weight loss compared to placebo – however, with a total of 2.9 kg lost weight compared to placebo over a year, the effect of orlistat was relatively small and gastrointestinal side effects were observed (Padwal et al., 2003). Therefore, the German clinical guidelines for prevention and therapy of obesity recommend to use orlistat only complementary to a basic therapeutic strategy which focuses on lifestyle changes and not as a therapeutic strategy on its own (Deutsche Adipositas-Gesellschaft (DAG) e.V. et al., 2014). Besides orlistat, incretins such as liraglutide – a glucagon-like peptide-1 receptor agonist which is mainly used in the treatment of type 2 diabetes – are approved for the treatment of obesity (Kretschmer, 2016). However, the approval of incretins for treatment of obesity took place quite recent, thus, these drugs are not taken into consideration in clinical guidelines for treatment of obesity in Germany yet.

As stated above, the consequences of non-treated obesity can be severe and the available therapeutic strategies – especially from a pharmacological point of view – are quite limited. Intriguingly, data published in the past 15 years suggested a novel therapeutic target to take on obesity: Brown Adipose Tissue (Cypess et al., 2009; Cypess et al., 2015; Liu et al., 2015; Virtanen et al., 2009).

1.2 Adipose Tissue

1.2.1 Types of adipose tissue and adipocytes

In general, two types of adipose tissues can be distinguished in mammals: Brown Adipose Tissue (BAT) and White Adipose Tissue (WAT) (Gesta et al., 2007). BAT is mainly known for its thermogenic properties. Key characteristics of brown adipocytes (BAs) are multiple small intracellular lipid droplets as well as a large amount of mitochondria containing uncoupling protein-1 (UCP1, thermogenin; see 1.2.2.1) (Cannon and Nedergaard, 2004).

WAT on the other hand is widely recognized for its ability to store energy. When high amounts of energy are available, e.g. after intake of high energy foods, white adipocytes (WAs) are able to store energy as triacylglycerol (TAG) and provide fuel during fasting periods (Cahill, 1976; Lafontan, 2005). With the discovery of leptin – a hormone secreted

by adipocytes which now is known to play a major role in food intake and energy balance (Obradovic et al., 2021) – around 30 years ago, it has also been established that WAT functions as an endocrine organ (Kershaw and Flier, 2004; Zhang et al., 1994). As stated in 1.1, an excessive amount of WAT – i.e. obesity – is also associated with different pathologies. It has been observed that overweight is associated with an increase in the expression levels of inflammatory cytokines such as tumor necrosis factor α in muscle as well as in adipose tissue in humans (Hotamisligil et al., 1995; Saghizadeh et al., 1996). This process of chronic inflammation promotes CVDs and such, highlighting the importance of WAT as an endocrine organ yet again (Hotamisligil, 2006; Mau and Yung, 2018; Serhan et al., 2008).

On a cellular basis, WAs characteristically carry unilocular lipid droplets and do not express UCP1, as shown in Figure 1 (Lafontan, 2005). Recent research has shown that even another type of adipocytes exists. Beige or brite (“brown in white”) adipocytes have been described as an intermediate cell type which have features of both BAs as well as WAs and express UCP1 (Wu et al., 2012). In this context, the process of browning has been described: upon specific stimuli, certain cell depots within WAT can take on a BAT-like phenotype and thereby become beige adipocytes (Himms-Hagen et al., 2000; Wu et al., 2013). Additional types of specialized adipocytes have also been described (e.g. the pink adipocyte in breast tissue), each playing a distinct role in mammalian physiology (Cinti, 2018).

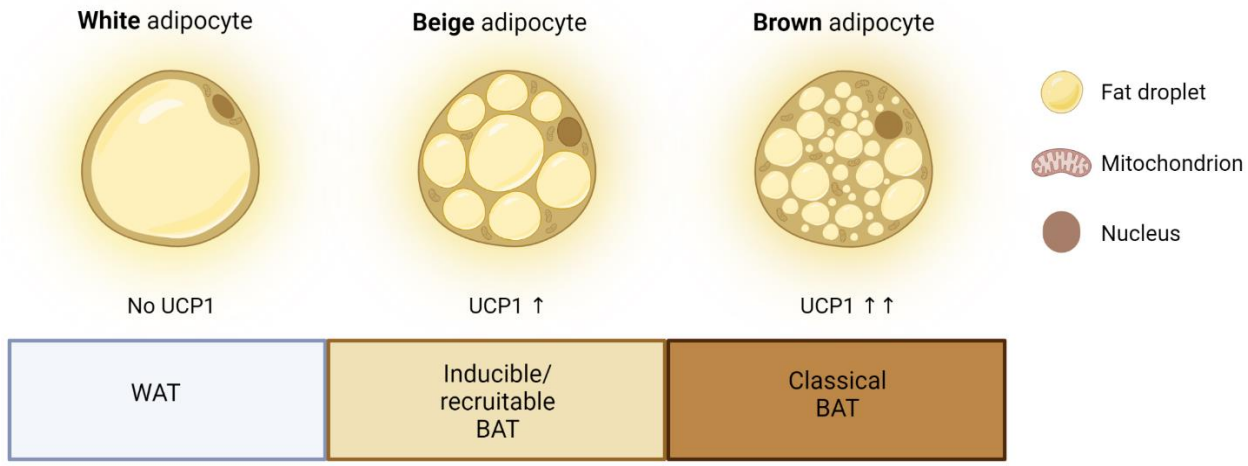

Figure 1: Distinct features of white, beige, and brown adipocytes.

White adipocytes characteristically carry a unilocular fat droplet and do not express UCP1. Brown adipocytes are characterized by high expression levels of UCP1, multilocular fat droplets as well as an extensive number of mitochondria. Beige/brite ("brown in white") adipocytes may be seen as an intermediate cell type between white and brown adipocytes. Beige adipocytes express lower levels of UCP1 than brown adipocytes and also carry less mitochondria. As shown, the lipid droplets of beige adipocytes are larger than the one in brown adipocytes, yet smaller than the ones in white adipocytes. Created with BioRender.com. Author's adaption from (Pfeifer and Hoffmann, 2015).

1.2.2 Brown adipose tissue

1.2.2.1 Anatomy and physiological function

During development, the central dermomyotome does not only give rise to muscle and skin, but also to BAT (Atit et al., 2006). BAT itself is a well vascularized tissue and is highly innervated by the sympathetic nervous system (SNS; Nnodim and Lever, 1988). It is composed of different types of cells such as endothelial cells, fibroblasts, immune cells and adipocytes. Its colour – and name – is due to its high amount of mitochondria containing iron and its high degree of vascularization (Cypess, 2022). BAT's major function consists of non-shivering thermogenesis (NST), a complex mechanism which protects the body against hypothermia in cold conditions (Foster and Frydman, 1978; Lindberg et al., 1967; van Marken Lichtenbelt et al., 2002). Cold is the physiological stimulus for BAT activation. Upon cold, the SNS releases norepinephrine (NE). NE activates BAs via β_3-adrenergic receptors. this leads to an increase in intracellular 3'-5'-cyclic adenosine monophosphate (cAMP), a second messenger which in turn stimulates protein kinase A (PKA). Finally, this leads to an increase in lipolysis (Cannon and

Nedergaard, 2004). Usually, an increase in lipolysis would result in an increase in oxidative phosphorylation and therefore elevated levels of adenosine triphosphate (ATP; Lardy and Ferguson, 1969). However, BAs carry a unique protein on their inner mitochondria membrane: UCP1 (Nicholls et al., 1978). UCP1 allows BAT to create energy by uncoupling the oxidative phosphorylation from ATP synthesis and thus contribute to maintaining normothermia (Cannon and Nedergaard, 2004).

Traditionally, it has been assumed that BAT only plays a role in rodents and human new-borns and not in human adults. However, recent evidence gathered by using ^{18}Fluorodeoxyglucose positron-emission tomographic and computed tomographic (^{18}F-FDG PET-CT) scans has shown that substantial amounts of active BAT exist in human adults (Cypess et al., 2009; Nedergaard et al., 2007; Virtanen et al., 2009). As shown in Figure 2, in human new-borns BAT can especially be found in the interscapular region. During aging, this depot of BAT atrophies (Heaton, 1972). In human adults it has been observed that metabolically active depots of BAT are mainly found in the supraclavicular and neck region, but also in the paravertebral, mediastinal, para-aortic, and suprarenal region. (Nedergaard et al., 2007). Similar to human new-borns, rodents mainly carry a large BAT-depot in their interscapular region. Additional smaller depots are found in the cervical, axillar, periaortic as well as perirenal regions (Cinti, 2000).

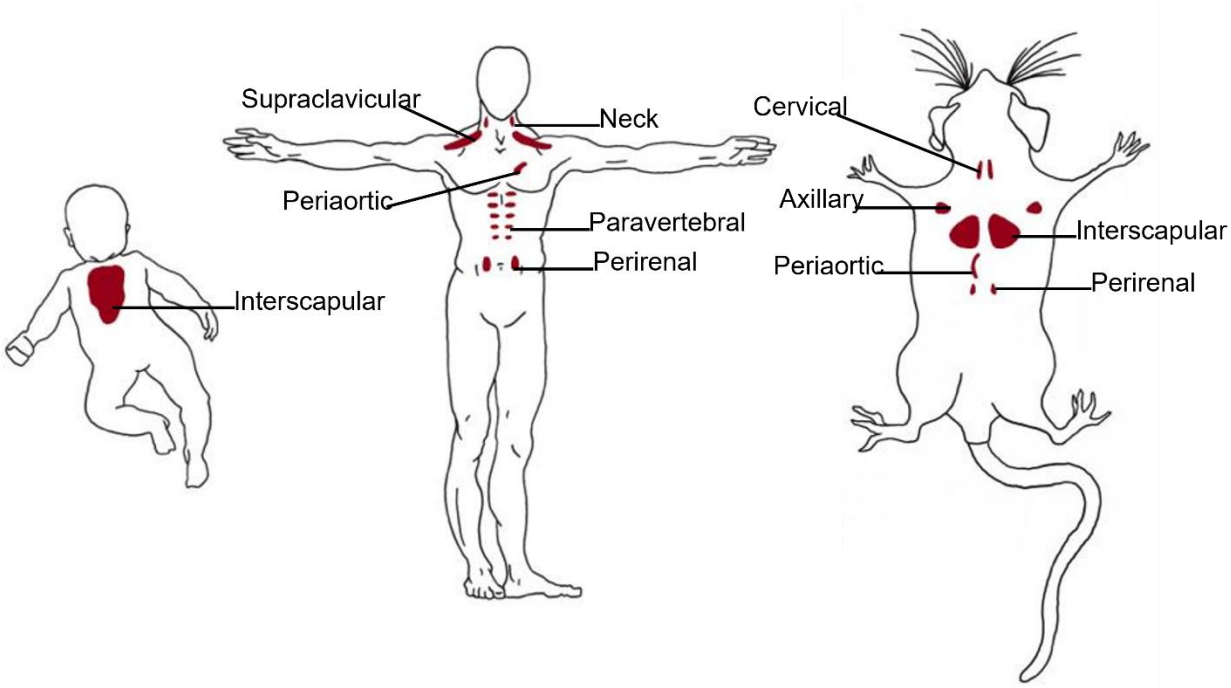

Figure 2: Anatomic locations of BAT in human newborns, human adults and rodents

Human new-borns carry a large depot of BAT in the interscapular region. In human adults, smaller depots of BAT can be found in the neck, supraclavicular, para-aortic mediastinal, paravertebral, and perirenal region. Rodents possess a larger depot of interscapular BAT as well as smaller depots in the cervical, axillary, periaortic and perirenal region. Author's adaption from (van den Berg et al., 2017).

1.2.2.2 Development and transcriptional control of brown adipocytes

As stated above (1.2.2.1), muscle and BAT share their origin to a certain extent. Furthermore, it was reported that the transcriptional signature of brown pre-adipocytes shares myogenic patterns. Intriguingly, even muscle-specific genes are expressed by brown pre-adipocytes (Timmons et al., 2007). Further supporting the evidence of a common heritage of BAs and myocytes , it has been shown that myogenic factor 5-positive precursor cells can differentiate into myoblasts as well as BAs, depending on the presence or absence of the transcriptional factor PRD1-BF1-RIZ1 domain containing 16 (PRDM16; Seale et al., 2008).

Peroxisome proliferator-activated receptor gamma (PPARγ) is considered to be the central transcriptional factor in adipogenesis (Rosen and MacDougald, 2006). During rat embryonic development, high expression levels of PPARγ can be detected in BAT on E18.5 (Braissant and Wahli, 1998). Another group of well-known transcriptional factors, which also play an important role in adipogenesis, are the CCAAT/Enhancer-binding-

proteins (C/EBPs; Rosen and MacDougald, 2006). For example, in BAT of mice lacking C/EBPβ and C/EBPγ, a decrease in lipid accumulation can be observed (Tanaka et al., 1997).

Prominent transcriptional factors, which especially influence the thermogenic adipose program and therefore play a major role in BA differentiation and UCP1 expression, are the aforementioned C/EBPβ and PRDM16 as well as peroxisome proliferator-activated receptor gamma coactivator 1-alpha (PGC-1α; Puigserver et al., 1998; Seale et al., 2007). Both PRDM16 and PGC-1α have been shown to be transcriptional co-activators of PPARγ (Puigserver et al., 1998; Seale et al., 2008). Although a number of important mechanisms in adipogenic and thermogenic differentiation have been decoded and described thoroughly, it appears the reality is even more complex. A frequently cited and surprising example for this was published in 2008 by Tseng et al., who showed how bone morphogenetic protein 7 (BMP7) influences BA differentiation (Tseng et al., 2008).

1.2.2.3 Brown adipose tissue as a therapeutic target for metabolic disorders

Pharmacological activation of BAT via β_3-adrenergic-receptors has been shown to ameliorate obesity in rodents (Collins et al., 1997; Yoshida et al., 1994). Since the rediscovery of active BAT in adult humans approximately 15 years ago, multiple studies were able to show an overall beneficial effect of activated BAT on body metabolism homeostasis. This includes an increase in plasma triglyceride clearance (Bartelt et al., 2011), improved glucose handling and insulin sensitivity (Chondronikola et al., 2014; Hanssen et al., 2015), as well as an overall increase in energy expenditure (Yoneshiro et al., 2013). A recent study also showed that BAT has a protective effect on cardiometabolic health in general (Becher et al., 2021).

With all these beneficial effects of activated BAT on metabolism, as well as the urgent need for new anti-obesity treatment (see 1.1), many clinical trials have emerged focusing on BAT as a therapeutic target. In these studies, unspecific β-agonists as well as specific β_3-agonists have been investigated (Buemann et al., 2000; Cypess et al., 2012). Unfortunately, especially unspecific sympathomimetic drugs either failed to activate BAT at all, or led to serious side effects (Carey et al., 2013; Cypess et al., 2012; Vosselman et al., 2012). However, in 2015 Cypess et al. published promising data on the subject,

showing that an oral intake of mirabegron – a specific β_3-adrenergic receptor agonist which is approved for treatment of overactive bladder – leads to a significant increase in energy expenditure, which was calculated to possibly yield in up to 10 kg weight loss within 3 years (Cypess et al., 2015; Hall et al., 2011). In general, mirabegron is known to cause less severe side effects than unspecific sympathomimetic drugs such as tachycardia, headache, nausea or diarrhoea (Herbel, 2023). This highlighted the role BAT might play in future obesity treatment once again.

1.3 CXCL12

1.3.1 Function

CXCL12 (CXC motif chemokine ligand 12, also known as SDF-1 [stromal-cell derived factor 1]) is a homeostatic chemokine (or chemotactic cytokine) which belongs to the group of CXC chemokines. Next to the group of CXC chemokines, three other groups of chemokines have been categorized: CC, XC, and CX_3C chemokines. The classification is based on the highly conserved NH_2-terminal cysteine group. Thus, in CXCL12 one different amino acid in between two cysteins can be found in the NH_2-terminus of the polypeptide (Zlotnik and Yoshie, 2000).

At first, CXCL12 was discovered as pre-B cell growth factor (PBGF; Nagasawa et al., 1994) and soon became known as SDF-1 (Nagasawa et al., 1996). In 1995 Shirozu et al. reported that the human gene for SDF-1 is located on chromosome 10q11 and that SDF-1 seems to be highly conserved in vertebrates (Shirozu et al., 1995). To date, six different isoforms of CXCL12 have been reported, all of which are derived from alternative splicing events (Yu et al., 2006).

Functionally, chemokines have been widely described for their role in leukocyte migration (Moser et al., 2004). The function of CXCL12 appears to be more complex and is mediated by two different receptors: CXCR4 (CXC motif chemokine receptor 4) and ACKR3 (atypical chemokine receptor 3; also known as CXCR7 [CXC motif chemokine receptor 7]; Balabanian et al., 2005; Oberlin et al., 1996). Global knockout of CXCL12 or of either receptor in mice is lethal (Gerrits et al., 2008; Ma et al., 1998; Nagasawa et al., 1996). However, the whole CXCL12-CXCR4-ACKR3 system does not only seem to play a major

role in physiological process such as angiogenesis, neurogenesis, lymphopoiesis, myelopoiesis, cardiogenesis etc. (Sadri et al., 2022), but also emerges to be an important factor in different pathologies such as AIDS (acquired immunodeficiency syndrome; Feng et al., 1996), inflammation (Yu et al., 2019) and different kinds of cancer (Barbieri et al., 2008; Meier et al., 2007).

CXCL12's function in cell migration, response to stimuli such as hypoxia, as well as its role in angiogenesis has been investigated using different types of cells such as endothelial cells, monocytes and cancer cells (Mirshahi et al., 2000; Schioppa et al., 2003). However, especially late research mainly focused on examining the role of CXCL12 in the context of tumor microenvironment. Meanwhile, studies examining the role of CXCL12 in adipose tissue are quite rare and mainly focus on CXCL12's role in WAT, WAT inflammation and obesity (Kim et al., 2014; Peng et al., 2016). It appears, the general understanding of the physiological role of CXCL12 in WAT is quite limited. However, even less studies have been published focusing CXCL12 in BAT.

In BAT, it was suggested that CXCR4 has a beneficial effect on thermogenic properties (Yao et al., 2014). Furthermore, Kurita et al. reported that CXCL12-signaling leads to BA differentiation (Kurita et al., 2019). For their studies, they also created a BAT-specific CXCR4 knock out mouse. To do so, UCP1 Cre mice were crossed with $CXCR4^{flox/flox}$ mice. These mice showed a decrease in insulin sensitivity compared to wild type mice (Kurita et al., 2019). Although these results seem quite promising, in general little is known about the role of CXCL12 in BAT and especially in BAT specific endothelial cells (ECs) .

1.3.2 Receptors and signalling

As stated above, CXCL12 is known to function by binding to CXCR4 and ACKR3. CXCR4, first discovered as leukocyte-derived seven-transmembrane domain receptor (LESTR; Loetscher et al., 1994), belongs to the superfamily of G protein-coupled receptors (GPCRs). GPCRs are seven transmembrane domain proteins, which can function in various ways in physiological conditions as well as disease (Hilger et al., 2018). Characteristically, GPCRs couple to a heterotrimeric G protein, which is made up of three different subunits: Gα, Gβ, and Gγ. In the inactive state, the G protein is bound to guanosine diphosphate (GDP). Upon activation, GDP dissociates from the Gα subunit and

is replaced by GTP (guanosine triphosphate), which allows the Gα subunit to dissociate from the Gβγ subunit and thus become active. Four different kinds of Gα subfamilies, each functioning in a distinct way, have been described (Wettschureck and Offermanns, 2005). $G\alpha_s$ and $G\alpha_{i/o}$ regulate adenylate cyclases (ACs), $G\alpha_{q/11}$ has an impact on phospholipase C (PLC) and $G\alpha_{12/13)}$ targets Rho-signalling (Hanlon and Andrew, 2015). Importantly, the Gβγ-complex can also function in several ways (Clapham and Neer, 1997).

A variety of different signalling pathways for the CXCL12-CXCR4 interaction have been described (Rubin, 2009). In 1997, Maghazachi reported that CXCR4 can couple to $G\alpha_{i/o}$ as well as $G\alpha_{q/11}$ in interleukin-2 activated natural killer cells (Maghazachi, 1997). Tan and colleagues showed, CXCR4 activation can also lead to $G\alpha_{12/13}$ signalling (Tan et al., 2006). However, it appears CXCR4 does not only act as a GPCR, but can also lead to JAK/STAT (Janus kinase/signal transducer and activator of transcription) activation (Vila-Coro et al., 1999). Furthermore, β-arrestin is also involved in CXCR4 function (Sun et al., 2002). Figure 3 gives an overview of the complex CXCL12 signalling as proposed by Janssens et al. (2018).

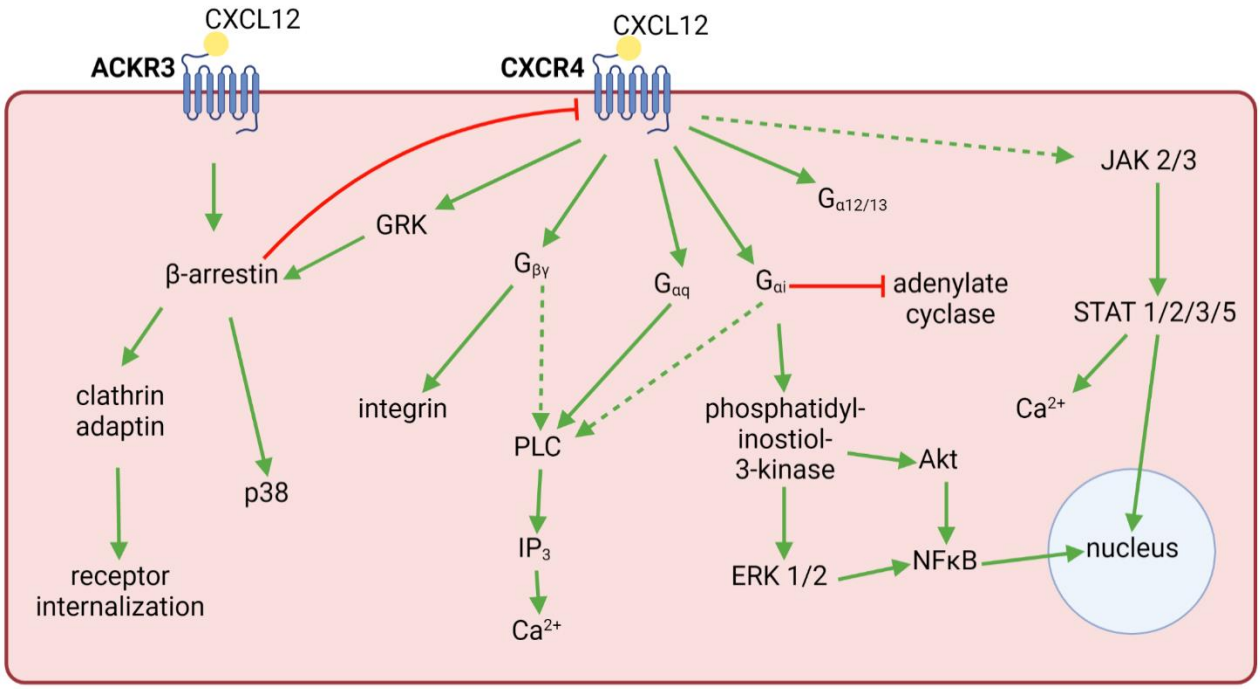

Figure 3: CXCL12 signalling

CXCL12 can influence a variety of intracellular mechanisms via CXCR4. By activating the JAK/STAT pathway it can have a direct impact on transcription. It can also impact integrins, calcium, phosphatidyl-inositol-3-kinase as well as inhibit adenylate cyclase. Activation of ACKR3 as well as CXCR4 impacts β-arrestin. β-arrestin mediates ACKR3's scavenger function and leads to receptor internalization. Green Arrows present primary pathways, dashed arrows present pathways without consensus in literature, red arrows present inhibitory pathways. ERK1/2 – extracellular signal-regulated kinase 1/2; GRK – G protein-coupled receptor kinase; IP3 – inositol-3-phosphate; JAK2/3 – Janus kinase 2/3; NFκB – nuclear factor kappa-light-chain enhancer of activated B-cells; PLC – Phospholipase C; STAT1/2/3/5 – signal transducer and activator of transcription. Created with BioRender.com. Author's adaption from (Janssens et al., 2018).

CXCL12 binds to ACKR3 with a higher affinity than to CXCR4 (Balabanian et al., 2005). Originally ACKR3 was especially known for its scavenging functions (Naumann et al., 2010). Different researchers were able to show that ACKR3 plays an important role in different physiological processes such as cardiogenesis and angiogenesis (Gerrits et al., 2008; Zhang et al., 2017). It was postulated that ACKR3 does not signal via G-proteins, but rather via β-arrestin, leading to an activation of MAP kinase (mitogen activated protein kinase) signaling (Rajagopal et al., 2010). These findings also led to ACKR3 being classified as an atypical chemokine receptor (Bachelerie et al., 2014). However, the claim that ACKR3 does not signal as a GPCR were challenged soon after, as Odemis et al. showed that ACKR3 activation leads to $G\alpha_{i/o}$ signalling in rodent astrocytes and human

glioma cells (Odemis et al., 2012). In summary, ACKR3's functional importance is well established while its molecular mechanisms need further investigation.

1.3.3 Clinical relevance

Ever since CXCR4 was discovered as a co-factor for HIV (human immunodeficiency virus) entry (Feng et al., 1996) and CXCL12 was found to be able to block HIV from entry into T-cells (Oberlin et al., 1996), clinical interest in the CXCL12-CXCR4-system has been high. Besides its relevance in HIV infection, a gain of function mutation in CXCR4 has been described to cause WHIM- (warts, hypogammaglobulinemia, infections, myelokathexis) syndrome (Kawai and Malech, 2009). With CXCL12's important function in cell-migration and angiogenesis, the CXCL12-CXCR4-axis has also been widely investigated in cancer research. Recent research suggests that CXCL12 as well as relative CXCL12-CXCR4 expression levels can serve as a prognostic parameter in colon cancers (Stanisavljević et al., 2016).

The CXCR4-antagonist plerixafor (also AMD3100), originally developed for the treatment of HIV infection, was discovered to mobilize hematopoietic cells from the bone marrow to the peripheral blood stream (Liles et al., 2005). In 2008, these findings finally led to the FDA approving plerixafor (Mozobil®) for the clinical use for mobilizing hematopoietic stem cells in order to perform autologous stem cell transplantation in patients suffering lymphoma and multiple myeloma (FDA, 2009).

1.4 Aim and research question

The pandemic of obesity keeps on rising and the need for new therapeutic strategies is urgent (see 1.1). BAT has been of high interest as a novel pharmacological target in treatment of obesity. However, our understanding of BAT biology still is limited. This thesis contributes to a growing body of literature focusing BAT.

Preliminary unpublished data of our lab showed that cold exposure – and therefore BAT activation – in mice upregulates CXCL12 messenger ribonucleic acid (mRNA) in BAT as well as in BAT-ECs significantly. Many researches have reported that CXCL12 plays an important role in EC function and angiogenesis, yet barely anything is known about either angiogenesis or the role of CXCL12 in BAT specifically. As proper vascularization of BAT is crucial for adequate supply of oxygen during thermogenesis, we decided to follow up the preliminary findings further, asking the leading question of this project:

- What is the role of CXCL12 in the crosstalk between microvascular ECs (MECs) and BAs?

In order to examine this question, the following research aims were formulated:

- Examine which stimuli lead to increased expression and secretion of CXCL12 in MECs and BAs.
- Investigate the function of CXCL12 in MECs and BAs.
- Investigate the function of CXCL12 in MEC-BA co-culture.
- Examine potential signalling pathways activated by CXCL12 in MECs and BAs.

To address these aims, *in vitro* experiments using murine BAs and murine MECs as a model to mimic BAT microcirculation were performed. First, BAs and muMECs were stimulated using NE. Furthermore, BAs and muMECs were exposed to hypoxic conditions. Effects of treatments were analysed using different methods such as real time quantitative polymerase chain reaction (RT-qPCR) and enzyme-linked immunosorbent assay (ELISA). In the following, a variety of functional assays such as proliferation assay, migration assay, and lipolysis assay were performed. Finally, the effect of CXCL12 in a

direct co-culture model of BAs and muMECs was analysed and second messengers such as cAMP were measured.

2. Materials and Methods

All chemicals used were obtained from Calbiochem (Darmstadt), Carl Roth GmbH (Karlsruhe), Merck (Darmstadt), Sigma-Aldrich (München) and VWR (Darmstadt). In case chemicals were purchased from other companies, it is specifically mentioned. For water purification, Milli-Q Water Purification System (Merck EMD Millipore) was used.

2.1 Cell culture

2.1.1 Materials

- µ-Slide 8 well (Ibidi GmbH, Cat. No. 80826)
- 10 cm^2 TC dishes, Standard (Sarstedt, Cat. No. 83.3902)
- 12-well TC plates (Sarstedt, Cat. No. 83.3921
- 24-well TC plates (Sarstedt, Cat. No. 83.3992.005)
- 3,3′,5-Triiodo-L-thyronine sodium salt (Sigma-Aldrich, Cat. No. T6397)
- 30 µM and 100 µM nylon meshes (Millipore, Cat. No. NY3002500, NY1H00010)
- 3-Isobutyl-1-methylxanthine (IBMX; Sigma-Aldrich, Cat. No. I5879)
- 6-well TC plates (Sarstedt, Cat. No. 83.3920)
- 96-well plates (Sarstedt, Cat. No. 83.3924)
- Autoclave, Varioklav 135 T (Faust)
- Bovine Serum Albumin (BSA; Sigma-Aldrich, Cat. No. A7030)
- Cannulas (Braun, Sterican 0,90 x 40 mm, Cat. No. 4657519)
- Centrifuge, Biofuge Primo (Heraeus)
- Collagenase, Type II (Worthington, Cat. No. CLS2)
- Conical tubes, 15 ml and 50 ml volume (Sarstedt, Cat. No. 62.554.502, 62.547.254)

- Countess Automated Cell Counter (Invitrogen, Cat. No. C10227)
- Cryogenic vials (Sarstedt, Cat. No. 72.379.992)
- Dexamethasone (Sigma-Aldrich, Cat. No. D4902)
- Dimethyl sulfoxide (DMSO; Roth, Cat. No. A994)
- Dulbecco's Modified Eagle's Medium (DMEM), high glucose, GlutaMAX(TM) (Gibco, Cat. No. 61965)
- Ethanol (EtOH; Roth, Cat.No. 9065.4)
- Fetal Bovine Serum (FBS; Biochrom, Cat. No. S0015)
- Gelatin solution 2 % (Inscreenex GmbH, Cat. No. INS-SU-1015-50ml)
- HEPES (Sigma-Aldrich, Cat. No. H7523)
- ProOx C21 Oxygen and Carbon Dioxide Subchamber Controller (BioSpherix, Ltd., RRID: SCR_021131)
- Incubator, HERAcell® 150 (Heraeus)
- Insulin solution human (Insulin; Sigma-Aldrich, Cat. No, I9278)
- L- (−)-Norepinephrine (+)-bitartrate salt monohydrate (Sigma-Aldrich, Cat. No. A9512)
- Laminar air flow, HerasafeTM (Heraeus)
- Microscope, LEICA DMIL (Leica Microsystems GmbH)
- Murine MEC (muMEC) medium (Inscreenex GmbH, Cat. No. INS-Cl-1004)
- Penicillin/streptomycin (P/S; Merck, Cat. No. A2213)
- Pipet-Lite XLS 2µl, 10µl, 20µl, 200µl, 1000µl (Rainin)
- Reaction tube 1.5 mL (Sarstedt, Cat. No. 72706)

- Recombinant mouse CXCL12 (R&D Systems, Cat. No. 460-SD)
- Scissors, forceps (Fine science tools)
- Serological pipettes 5ml, 10ml, 25ml (Sarstedt, Cat. No. 86.1253.001, 86.1254.001, 86.1685.001)
- Syringe filter 0.22 µm (VWR, Cat. No. 514-0061)
- Syringes 5 mL (BD Discardit II, Cat. No. 309050)
- T175 tissue culture flasks (Sarstedt, Cat. No. 83.3912.002)
- TC-Insert 12 well plate, pore size 3 µm (Sarstedt, Cat. No. 83.3931.300)
- Trypan Blue Stain (Gibco, Cat. No. 15250)
- Trypsin-EDTA (0.05 %), phenol red (Trypsin; Gibco, Cat. No. 25300054)
- Water bath (Memmert GmbH)

2.1.2 Cell culture of murine BA

2.1.2.1 Isolation and immortalization of BAT-derived brown preadiopcytes

In order to isolate murine brown preadiopcytes, the interscapular BAT was dissected from neonatal C57Bl6-J mice and transferred into a 1.5ml reaction tube containing 0.5 ml isolation buffer (see Table 1). While the samples were located in the reaction tube, the tissue was cut into small pieces using the surgical scissors. Next, the suspension was transferred into a 15 ml conical tube containing 3 ml of isolation buffer. Afterwards, the samples were incubated in a water bath at 37 °C and shaken thoroughly every 5 minutes. After 30 minutes of incubation, the suspension was filtered through a 100 µm nylon mesh and put on ice for 30 minutes. Using a syringe and cannula, 2 ml of the middle phase was collected and filtered through a 30 µm nylon mesh. The suspension was centrifuged for 10 minutes at 700 g and the resulting pellet was re-suspended using 2 ml of BA culture medium (Table 2). In the following, the suspension was plated into a 6-well TC plate and incubated for 24 hours at 37 °C and 5 % CO_2. After 24 hours of incubation, the media was

aspirated and the cells were immortalized by adding 800 µl of BA growth medium (Table 3) containing a lentivirus expressing the Simian Virus 40 (SV40) large T-antigen at a dose equivalent to 200 ng of reverse transcriptase. Isolation and immortalization of cells was performed by Markus Raspe.

Table 1 BA isolation buffer

Substances were dissolved in H_2O and sterile filtered. The pH was adjusted to 7.4 using NaOH. BSA and collagenase were added right before use.

Substances	Quantity
NaCl	123 mM
KCl	5 mM
$CaCl_2$	1.3 mM
HEPES	100 mM
BSA	1,5 %
Collagenase II	2 mg/ml

Table 2 BA culture medium

Substances were dissolved in DMEM, high glucose (Gibco, Cat. No. 61695).

Substances	Quantity
FBS	10 %
HEPES	10 nM
Insulin	4 nM
P/S	1 %
Sodium-Ascorbat	25µg/ml
T3	4 nM

Table 3 BA growth medium

Supplements were added to DMEM, high glucose (Gibco, Cat. No. 61695).

Substances	Quantity
FBS	10 %
P/S	1 %

2.1.2.2 Expansion and freezing of immortalized brown preadipocytes

In order to expand the cells, immortalized brown preadipocytes were seeded onto 10 cm^2 TC dishes in 10 ml of BA growth medium. The media was changed every other day until the cells covered ~80-90 % of the 10 cm^2 TC dish. Cell growth was monitored using an inverted light microscope. At 80-90 % confluency, the cells were washed twice with PBS (Table 4). Next, 2 ml of Trypsin-EDTA was added per 10 cm^2 TC dish and the cells were incubated for 3 minutes at 37 °C. After 3 minutes of incubation, 8 ml of BA growth medium was added and the cell suspension was transferred into a 15 ml conical tube. The suspension was centrifuged for 8 minutes at 1000 rpm. After, the pellet was re-suspended in BA growth medium and the amount of cells was counted using Countess Automated Cell Counter. In order to count the cells, 10 µl of cell suspension was mixed with 10 µl of trypan blue stain. 10 µl of the resulting mix was pipetted into a Countess Cell Counting Chamber Slide. Following, cells were either plated onto 10 cm^2 TC dishes for expansion (in a ratio of 1:10) or frozen. For freezing, cells were suspended in BA growth medium containing 10 % DMSO and aliquoted into cryogenic vials. Frozen cells were stored at -80 °C for 24 hours. For long time storage, the cryogenic vials were transferred to a -150°C freezer. Brown preadipocytes in passage 4 were used to perform experiments.

Table 4 Phosphate buffered saline (PBS)

Compounds were added to dH2O to a total volume of 1000 ml. ThepH was adjusted to 7.4 using NaOH. After, the solution was autoclaved for 20 minutes at 121°C.

Substances	**Quantity**
NaCl	137 mM
KCl	2.7 mM
Na_2HPO_4	8 mM
KH_2PO_4	1.4 mM

2.1.2.3 Differentiation of brown preadipocytes

In order to perform *in vitro* experiments, brown preadipocytes were seeded (~80.000 cells/12-Well; ~160.000 cells/6-Well) in BA growth medium and incubated at 37 °C and 5 % CO_2 until 100 % confluency. When confluent (= D-2), the media was changed to BA differentiation medium (Table 5). After two more days of incubation (on D0), the media

was changed again to BA induction medium (Table 6) in order to induce BA differentiation. The cells were incubated in induction media for two days. On D2, the media was changed back to BA differentiation media. Cells were cultured in BA differentiation media until D7, the media was renewed on D4 and D6. When not further specified, experiments were performed with differentiated BAs (D7 of differentiation protocol).

Table 5 BA differentiation medium

Supplements were added to DMEM, high glucose (Gibco, Cat. No. 61695).

Substances	Quantity
FBS	10 %
P/S	1 %
Insulin	1 nM
T3	20 nM

Table 6 BA induction medium

Supplements were added to BA differentiation medium (Table 5).

Substances	Quantity
Dexamethasone	1 µM
IBMX	0.5 nM

2.1.3 Culture of murine microvascular endothelial cells

Murine microvascular endothelial cells were purchased from Inscreenex GmbH. Before plating the cells, culture dishes were coated with PBS containing 0.5 % gelatine for 30 minutes at 37 °C. For experiments, muMECs were seeded on 12 well plates (60.000 cells/well) or 6 well plates (120.000 cells/well) and grown to 100 % confluency. For expansion, muMECs were seeded on T-175 cm^2 flasks at a density of 10.000 cells/cm^2. Expansion and freezing of muMECs was performed as described in 2.1.2.2. For muMECs, muMEC media was used (Table 7).

Table 7 microvascular endothelial cell medium

Supplements were added to basal muMEC media (Inscreenex GmbH, Cat. No. INS-ME-1004).

Substances	Quantity
muMEC supplement	5 %
P/S	1 %

2.1.4 Co-culture of BAs and muMECs

2.1.4.1 Transwell system

BAs were seeded in 12 well plates and differentiated as described in 2.1.2.3. While BAs were differentiated, muMECs were seeded in TC inserts (for 12 well plates, pore size 3 µm; 20.000 cells/insert) and grown to confluency. On D6 of the BA differentiation protocol, the TC inserts containing muMECs were transferred to the BA and treated with NE. The transwell system was incubated for 24 hours at 37 °C and 5 % CO_2. After incubation, cells were harvested for further read-outs.

2.1.4.2 Direct co-culture

BAs were seeded in 6 well plates and differentiated (see 2.1.2.3). Meanwhile muMECs were also seeded in 6 well plates and grown to confluency. On D5 of the BA differentiation protocol, muMECs and BAs were detached from the plate using trypsin (0.8 ml/6 well). While trypsinizing, cells were incubated for three minutes at 37 °C. In order to deactivate the trypsin, 2 ml of BA differentiation media (Table 5) were added per well. In order to mix muMECs and BAs, the cell suspension of one 6 well each was transferred to a 15 ml conical tube. Afterwards, the cell suspension was centrifuged for 8 minutes at 1000 rpm. The supernatant was aspirated and the pellet was re-suspended using BA differentiation media. Cells were then re-seeded either in 8-well µ-slides (Ibidi) or 12 well plates. In order to allow the cells to attach to the culture dish, the co-culture was incubated for 6 hours. After, cells were treated with the drug of interest and then incubated for another 48 hours at 37 °C and 5 % CO_2. After incubation, cells were either fixed and stained for Endomucin and nuclei (see 2.2 for Endomucin stain and 2.12 for Hoechst nuclei stain) for microscopy or harvested for mRNA-isolation.

2.2 Endomucin stain

The following list provides an overview of materials used. Disposables, pipettes etc. used are listed in 2.1.1.

- µ-Slide 8 well (Ibidi GmbH, Cat. No. 80826)
- Axio Observer (Carl Zeiss AG, Oberkochen, Germany)
- Bovine Serum Albumin (Sigma-Aldrich, Cat. No. A7030)
- Colibri 7 (Carl Zeiss AG, Oberkochen, Germany)
- Goat Anti-Rabbit IgG H&L (Abcam, Cat. No. ab150077)
- Mouse Endomucin Antibody (R&D Systems, Cat. No. AF4666)
- Paraformaldehyde (PFA; Roth, Cat. No. 0335.3)
- PBS (Table 4)
- Tween®-20 (Carl Roth GmbH & Co. KG, Cat. No. 9127.1)

In order to stain muMECs, the cells were washed with PBS (Table 4) twice. After, cells were fixed by adding 4 % PFA in PBS (200 µl per well of a 8 well µ-slide; Table 8) and incubated for 15 minutes at room temperature (RT). Following fixation, cells were washed with PBS yet again. After, 200 µl of permeabilization buffer (Table 9) were added per well and incubated at RT for 20 minutes. After incubation, permeabilization buffer was aspirated and cells were incubated with blocking buffer (Table 11) for 60 minutes at RT. Next, mouse endomucin antibody was diluted 1:100 in blocking buffer and added to the wells. Another incubation step at 4 °C overnight followed. On the next day, cells were washed three times for 5 minutes using PBS-T (Table 10). The secondary antibody was diluted 1:500 in blocking buffer, added to the wells and yet again incubated at RT for 60 minutes. Afterwards, the washing steps described previously were repeated and cells were imaged directly or stored at 4 °C protected from light. In case of storage, 100µl PBS was added per well and the slides were imaged within seven days of staining. For imaging,

Axio Observer was used and pictures were acquired at 475 nm with the following settings: Intensity: 50 %, Exposure: 50 ms.

Table 8 4% paraformaldehyde in PBS

PFA was added to PBS and dissolved by stirring at 55°C. When completely dissolved, PFA was stored at 4°C.

Substances	Quantity
PFA	40 g
PBS	960 ml

Table 9 Permebealization buffer

Tween®-20 was added to PBS and stirred at RT until homogenized. Buffer was stored at 4°C.

Substances	Quantity
Tween®-20	3 ml
PBS	997 ml

Table 10 PBS-T

Tween®-20 was added to PBS and stirred at RT until homogenized. Buffer was stored at 4°C.

Substances	Quantity
Tween®-20	1 ml
PBS	999 ml

Table 11 Blocking buffer

BSA was added to PBS-T and put on a roller until homogenized. Buffer was stored at 4°C.

Substances	Quantity
BSA	1 g
PBS-T	99 ml

2.3 Oil red O staining

The following list provides an overview of materials used. Disposables, pipettes etc. used are listed in 2.1.1.

- 2-Propanol (Roth, Cat. No. 6752.4)
- Folded filters 240 mm (GE Healthcare Life Sciences, Cat. No. 10311651)
- Oil Red O (Sigma-Aldrich, Cat. No. O9755)
- Paraformaldehyde (Roth, Cat. No. 0335.3)
- PBS (Table 4)

Oil red O staining was performed in order to stain for lipid droplets in mature BAs. First, cells were fixed in a 6 well plate using 4 % PFA as described in 2.2. Ready to use oil red O solution (Table 12) was filtered twice, using a paper filter. 800 µl of the filtered solution were added per 6 well and incubated for three hours at RT. After incubation, the red O solution was washed of carefully using dH_2O. Plates were then put onto paper towel and allowed to dry at RT. Pictures were acquired using a conventional office scanner.

Table 12 Oil Red O

Chemicals for the stock solution were mixed and stirred overnight at RT. For staining, the stock solution was diluted with dH_2O in a ratio of 3:2 and filtered twice using paper filters. Stock solution was stored at RT, ready to use solution was prepared freshly before usage and disposed after.

Substances	**Quantity**
Stock solution	
Oil Red O	500 mg
Isopropanol	100 ml
Ready to use solution	
Red O stock solution	60%
dH_2O	40%

2.4 Quantification of intracellular cAMP

The following list provides an overview of materials used. Disposables, pipettes etc. used are listed in 2.1.1.

- 3-Isobutyl-1-methylxanthine (IBMX; Sigma-Aldrich, Cat. No. I5879)
- Direct cAMP ELISA Kit (Enzo Life Sciences, Inc., Cat. No. ADI-900-066)

- Enspire® microplate reader (Perkin Elmer, Cat. No. 2300-0000)
- L-(−)-Norepinephrine (+)-bitartrate salt monohydrate (Sigma-Aldrich, Cat. No. A9512)
- Recombinant mouse CXCL12 (R&D Systems, Cat. No. 460-SD)
- PBS (Table 4)

Intracellular cAMP of either muMECs or differentiated BAs (D7 of differentiation protocol, see 2.1.2.3) was analysed. Prior to treating the cells with different compounds, an incubation step for 30 minutes at 37 °C and 5 % CO_2 with media containing 0.5 nM was performed. After, the compound of interest was added directly into the well. Cells were incubated for another 10 minutes (37 °C, 5 % CO_2) and then washed with PBS once. In the following, cells were lysed using 0.1 M HCl and transferred into 1.5 ml reaction tubes. Intracellular cAMP levels were determined using the direct cAMP ELISA-Kit provided by Enzo. The manufacturer's instructions were followed precisely. Finally, using an Enspire® microplate reader, the optical density at 405 nm was measured and intracellular cAMP concentrations were calculated using a four parameter-logistic equation. Lastly, the protein content in the cell lysate was determined using Bradford assay (2.6) and cAMP concentrations were normalized to protein content.

2.5 Analysis of CXCL12 in cell culture supernatant

The following list provides an overview of materials used. Disposables, pipettes etc. used are listed in 2.1.1.

- Enspire® microplate reader (Perkin Elmer, Cat. No. 2300-0000)
- L-(−)-Norepinephrine (+)-bitartrate salt monohydrate (Sigma-Aldrich, Cat. No. A9512)
- PBS (Table 4)
- ProOx C21 Oxygen and Carbon Dioxide Subchamber Controller (BioSpherix, Ltd., RRID: SCR_021131)

- Quantikine® ELISA mouse CXCL12/SDF-1α (R&D systems; Cat. No. MCX120)

Using a CXCL12 ELISA provided by R&D systems, the amount of CXCL12 secreted by differentiated BAs (see 2.1.2.3) or muMECs was determined. Prior to the assay, cells were washed with PBS once. After, the cells were incubated in starved BA differentiation (Table 13) or starved muMEC media (Table 14) respectively. Cells were then either treated with the substance of interest or exposed to hypoxia (1% O_2) and incubated at 37 °C and 5 % CO_2. After incubation, the supernatant was transferred to a 15 ml conical tube, centrifuged at 300 g for 5 minutes and once again transferred to a 1,5 ml reaction tube. As recommended by the manufacturer, the supernatant was then diluted in a ratio of 1:10 before performing the assay. Next, the Quantikine® ELISA mouse CXCL12 provided by R&D systems was performed. The manufacturer's instructions were followed precisely. Optical density at 450 nm and 540 nm was measured using a microplate reader. The optical density at 540 nm was subtracted from 450 nm. CXCL12 concentrations were calculated using a four parameter-logistic equation. In order to normalize CXCL12 to protein amount, the protein of the cells was isolated and protein concentration was determined as described in 2.6.

Table 13 Starved BA differentiation medium

Supplements were added to DMEM, high glucose (Gibco, Cat. No. 61695).

Substances	Quantity
P/S	1 %
Insulin	1 nM
T3	20 nM

Table 14 Starved muMEC medium

Substances	Quantity
muMEC media	99 ml
P/S	1 ml

2.6 Isolation and quantification of protein

The following list provides an overview of materials used. Disposables, pipettes etc. used are listed in 2.1.1.

- BioPhotometer D30 (Eppendorf)
- Cell scraper (Labomedic, Cat. No. 2015217)
- Centrifuge 5430R (Eppendorf)
- Complete protease inhibitor cocktail (Complete® EDTA free; Roche, Cat. No. 04693116001)
- Coomassie brilliant blue G-250 (Merck, Cat. No. 1.15444.0025)
- Deoxycholic acid sodium salt (Roth, Cat. No. 3484.2)
- Minispin centrifuge (Sigma-Aldrich, Cat. No. Z606235)
- Nonidet® P 40 Substitute (NP-40; Fluka BioChemika, Cat. No. 74385
- PBS (Table 4)
- Sodiumchloride (Roth, Cat. No. 3957.1)
- Sodium dodecyl sulphate (SDS; Roth, Cat. No. 2326.2)
- Sodiumflouride (NaF; Roth, Cat. No. 2618.1)
- Sodium orthovanadate (Na_3VO_4; Roth, Cat. No. 0735.1)
- Tris HCl (Roth, Cat. No.9090.3)
- Ultrasonic bath (Bandelin)

In order to isolate protein, cells were washed with PBS once. Cell lysis buffer (Table 15; Table 16) was added into the well (200 µl per 6 well, 100 µl per 12 well) and cells were scrapped off the plate using a cell scraper. After, cells were transferred into a 1.5 ml reaction tube and put into an ultrasonic bath for 45 seconds. Next, the samples were

centrifuged for 20 minutes at 13000 rpm and 4°C. In the following, the middle phase (containing the protein) of the reaction tube, was transferred to a fresh reaction tube and stored on ice. Protein concentration was either determined right away or samples were stored at -80 °C.

For protein quantification, Bradford assay was performed. 2 µl of the isolated protein suspension were added to 98 µl 0.15 M NaCl. 1 ml of Bradford reagent (Table 17) was added and incubated for 1 minute at RT. Protein concentration was determined by measuring the samples' absorbance at 595 nm using a BioPhotometer and a BSA standard calibration curve with known protein concentrations.

Table 15 Radioimmunoprecipitation assay buffer (RiPA)

Substances were dissolved in ddH_2O and sterile filtered. Buffer was stored at 4°C.

Substances	Quantity
Deoxycholic acid sodium salt	0.5 %
NaCl	150 mM
NP-40	1.0 %
SDS	0.1 %
Tris HCl	50 mM

Table 16 Lysis buffer

Substances were added to RiPA buffer (Table 15) right before use.

Substances	Quantity
Complete® EDTA free	40 µl/ml
NaF	10 mM
Na_3VO_4	1 mM

Table 17 Bradford reagent

Substances were dissolved in ddH_2O, stirred overnight and filtered through a paper filter. The solution was stored at 4°C.

Substances	Quantity
Coomassie brilliant blue G250	0.01 %
EtOH	5 %
H_3PO_4	8.5 %

2.7 Isolation and quantification of RNA

The following list provides an overview of materials used. Disposables, pipettes etc. used are listed in 2.1.1.

- 2-Propanol (Roth, Cat.No. 6752.4)
- Centrifuge (Eppendorf, Cat. No. 5415R)
- Chloroform (Roth, Cat.No. 6340.1)
- Diethylpyrocarbonate (DEPC; Roth, Cat. No. K028.1)
- Ethanol (Roth, Cat.No. 9065.4)
- NanoDrop 2000 Spectrophotometer (ThermoScientific)
- PBS (Table 4)
- RNA Reagent (IST Innuscreen GmbH, Cat. No. 31-01117)
- Thermomixer comfort (Eppendorf, Cat. No. 2050-120-04)
- Vacuum centrifuge, Concentrator plus (Eppendorf, Cat. No. 5305YP609431)
- Vortex (Merck Eurolab, Cat. No. MECB1719)

In order to isolate RNA, cells were washed with PBS once. 1 ml of cold RNA reagent (stored at 4 °C) was added per well in order to lyse the cells. Next, the cell lysate was transferred to a 1.5 ml reaction tube. 200 µl of ice cold chloroform (stored at -20 °C) was

added. Samples were mixed gently for 15 seconds and incubated at RT for 5 minutes. In the following, the samples were centrifuged at 13000 rpm and 4 °C for 20 minutes. After centrifugation, 500 µl of the upper clear phase – containing the RNA – were transferred to a fresh 1.5 ml reaction tube using a pipette. 500 µl of 99 % 2-Propanol were added. Samples were mixed carefully yet again. Again the samples were centrifuged: 10 minutes at 13000 rpm and 4 °C. After centrifugation, the supernatant was discarded and the resulting pellet was washed twice. For washing, 1 ml of 75 % EtOH was added, samples were vortexed briefly and centrifuged for 10 minutes at 13000 rpm and 4°C. After the final washing step, to concentrate RNA, samples were centrifuged in Eppendorf Concentrator plus for 25 minutes at 30 °C, mode was set to V-AL. After drying, the pellet was dissolved by adding 20-30 µl DEPC-H_2O (Table 18; volume depending on the amount of cells used for RNA isolation) per sample. Samples were then put on a thermomixer at 500 rpm and 55°C for 10 minutes. When the RNA was dissolved, Nanodrop 2000 Spectrophotometer was used to determine the final RNA concentration. RNA was then used for further experiments or stored at -80 °C.

Table 18 Diethylpyrocarbonate (DEPC)-H_2O

DEPC was added to H_2O. Protected from light, the mixture was stirred over-night and autoclaved twice in the following. DEPC-H_2O was stored at RT.

Substances	Quantity
DEPC	0.1 %
H_2O	99.9 %

2.8 Synthesis of complementary DNA (cDNA)

The following list provides an overview of materials used. Disposables, pipettes etc. used are listed in 2.1.1.

- 0.5 ml reaction tube (Sarstedt, Cat. No. 7.2.699)
- Protoscript® II First Strand cDNA Synthesis Kit (New England BioLabs, Cat. No. E6560S)
- Thermocycler Biometra TOne (Analytik Jena)

To synthesize cDNA, Protoscript® II First Strand cDNA Synthesis Kit was used. First, RNA was isolated and concentration was measured as described in 2.7. According to the manufacturer's instructions, reaction mixes were pipetted as shown in Table 19. Per sample a maximum of 6 µl containing 1 µg RNA was used for cDNA synthesis (in case RNA concentration did not allow to use 1 µg of RNA, either 500 ng or 250 ng RNA per sample were used). Next, a Thermocycler Biometra TOne was used for incubation. The program used is shown in Table 20. After incubation, the cDNA was either used for downstream applications or stored at -20 °C.

Table 19 Reaction set up for cDNA Synthesis

Substances	**Quantity**
RNA	Up to 6 µl
Random Primer Mix	2 µl
Photoscript II Reaction Mix (2x)	10 µl
Photoscript Enzyme Mix (10x)	2 µl
Nuclease-free H_2O	To total volume of 20 µl

Table 20 Thermocycler program for cDNA synthesis

Step	**Temperature**	**Time**
1	25 °C	5 minutes
2	42 °C	60 minutes
3	80 °C	5 minutes
4	4 °C	∞

2.9 Real Time Quantitative Polymerase Chain Reaction (RT-qPCR)

The following list provides an overview of materials used. Disposables, pipettes etc. used are listed in 2.1.1.

- Electronic pipettes, E4 XLS and XLS+ (Rainin)
- MicroAmp™ Optical 384-Well Reaction Plate (Thermo Fisher, Cat. No. 4343370)
- Real-time PCR machine, HT7900 (Applied Biosystems)
- SYBR-Green PCR master mix (Applied Biosystems, Cat. No. 4309155)

In order to examine mRNA expression levels of different genes, RNA from cells was isolated, cDNA was synthesized (see 2.7; 2.8) and RT-qPCR was performed. Prior to RT-qPCR, the cDNA was diluted in a ratio of 1:20 (when 1 µg RNA was used for synthesis) or 1:10 (when less RNA was used for cDNA synthesis). Per well in an MicroAmp™ Optical 384-Well Reaction Plate, 5 µl SYBR-Green PCR master mix, 0.5 µl of primer (forward and reverse; concentration: 100 µM) and 4 µl of diluted cDNA were added. Relative gene expression levels were calculated using hypoxanthine-guanine phosphoribosyltransferase (Hprt) as an internal standard. Each sample was pipetted in duplicates and for each primer set a negative control containing ddH_2O instead of cDNA was run. A melting curve was run and analysed in order to control the quality of the RT-qPCR product. Primer sequences are shown in Table 21. The RT-qPCR reaction program was set up as shown in Table 22.

Table 21 Primer sequences

Primers were designed using PubMed and ordered from Microsynth AG. Primers were diluted in nuclease free water according to manufacturer's instructions.

Gene	Sequence forward	Sequence reverse
Ackr3	GACTCAAGGAGCAGGTCACT	TGGCCAGTTGATGTCAGAGT
Cxcl12	GTTCTTCGAGAGCCACATCG	CTTCAGCCGTGCAACAATCT
Cxcr4	AAACCTCTGAGGCGTTTGGT	GGAAGCAGGGTTCCTTGTTG
Elovl3	CTGGGTACTCTGAGGATGTGG	TGGACAAAGATGAGTGGACGC
Fabp4	GCGTGGAATTCGATGAAATCA	CCCGCCATCTAGGGCTAGGGTTATGA
Hif1α	ACAGAGCCGGCGTTTAGG	CGACGTTCAGAACTCATCCTATTTT
Hif2α	TACTAAGTGGCCTGTGGGTG	AGTCCTTTGCAGACCTCATCT
Hprt	GTCCCAGCGTCGTGATTAGC	TCATGACATCTCGAGCAAGTC
Ucp1	GGATGGTGAACCCGACAACT	CCTTGGATCTGAAGGCGGAC

Table 22 RT-qPCR program

Steps 2 and 3 were repeated for 40 cycles.

Step	Temperature	Time
1	95°C	600 seconds
2	95°C	15 seconds
3	60° C	60 seconds
Melting curve		
4	95°C	15 second
5	60°C	60 seconds
6	95°C	15 seconds

2.10 Lipolysis assay

The following list provides an overview of materials used. Disposables, pipettes etc. used are listed in 2.1.1.

- Bovine serum albumin (Sigma-Aldrich, Cat. No. A7030)
- DMEM (Gibco, Cat. No. 21063)
- Enspire® microplate reader (Perkin Elmer, Cat. No. 2300-0000)
- Free glycerol reagent (Sigma-Aldrich, Cat. No. F6428)
- Glycerol standard (Sigma-Aldrich, Cat. No. G7793)
- L- (−)-Norepinephrine (+)-bitartrate salt monohydrate (Sigma-Aldrich, Cat. No. A9512)
- Recombinant mouse CXCL12 (R&D Systems, Cat. No. 460-SD)

Lipolysis medium was made by adding 2 % BSA to DMEM. Differentiated BAs (D7 of differentiation protocol, see 2.1.2.3) were washed with lipolysis medium twice. Subsequently, 300 µl lipolysis medium was added per 12 well and compounds of interest were added. Cells were then incubated for 2 hours at 37 °C and 5 % CO_2. After incubation, 40 µl of every sample was pipetted into a 96 well plate in duplicates, 40 µl of fresh lipolysis medium were used as a blank. 60 µl of free glycerol reagent were added. For the standard, 5 µl of glycerol standard was pipetted into a well and 95 µl of free glycerol reagent was added. An incubation step for 5 minutes at 37 °C followed. An Enspire® microplate reader was used to determine the optical density at 540 nm. Optical density at 600 nm was used as a reference. Total glycerol content was calculated using the determined absorbance values and the following formula:

$$Glycerol\ content = \frac{sample - blank}{standard - blank} * standard\ concentration$$

Glycerol content was normalized to protein (protein was isolated and quantified as described in 2.6).

2.11 Cell migration assay

The following list provides an overview of materials used. Disposables, pipettes etc. used are listed in 2.1.1.

- Countess Automated Cell Counter (Invitrogen, Cat. No. C10227)
- Enspire® microplate reader (Perkin Elmer, Cat. No. 2300-0000)
- PBS (Table 4)
- QCM™ 24-Well Colorimetric Cell Migration Assay (Merck, Cat. No. ECM 508)
- Trypan Blue Stain (Gibco, Cat. No. 15250)

muMECs were seeded in a 10 cm^2 TC dish and incubated at 37 °C and 5 % CO_2 two days prior to performing the assay (for detailed description of muMEC cell culture method see 2.1.3). 24 hours after seeding, cells were washed with PBS once and starved medium was added (Table 14). Cells were incubated for another 24 hours until around 70-80 % confluency. The cells were then washed with PBS and 2 ml of trypsin was added. Cells were then incubated at 37 °C and 5 % CO_2 for 3 minutes. When detached from the culture dish, cells were transferred to a 15 ml conical tube and counted using Countess automated cell counter and trypan blue stain (for details see 2.1.2). Afterwards, cells were centrifuged at 300 g for 4 minutes and re-suspended in starvation medium. A 24 well plate with inserts for cell migration was prepared. Each insert was filled with 300 µl cell suspension containing a total of 150.000 cells. The compounds of interest were added in starvation medium into the bottom well. The muMECs were then incubated for 8 hours at 37 °C and 5 % CO_2. Further, the assay was performed following the manufacturer's instructions. Using an Enspire® microplate reader, the optical density at 560 nm was determined.

2.12 Proliferation assay

The following list provides an overview of materials used. Disposables, pipettes etc. used are listed in 2.1.1.

- Axio Observer (Carl Zeiss AG, Oberkochen, Germany)

- Bovine Serum Albumin (Sigma-Aldrich, Cat. No. A7030)
- Click-iT® EdU Alexa Fluor® 488 Imaging Kit (Invitrogen, Cat. No. C10337)
- Colibri 7 (Carl Zeiss AG, Oberkochen, Germany)
- ImageJ (Schneider et al., 2012)
- Paraformaldehyde (Roth, Cat. No. 0335.3)
- PBS (Table 4)
- Triton-X-100 (Prolabo, Cat. No. 28 817.295)

In order to analyse proliferation in muMECs, a Click-iT® EdU-Kit was used. 20.000 muMECs were seeded per well in a µ-Slide 8 well and incubated for 16 hours at 37 °C and 5 % CO_2 (for a detailed description of muMEC cell culture see 2.1.3). Everything was performed in duplicates. Following this, muMECs were washed with PBS once. Compounds of interest and EdU were added to starvation medium (Table 14). 200 µl of the resulting mix were added per well and cells were incubated for another 8 hours (37 °C; 5 % CO_2). According to manufacturer's instructions, the cells were then fixed using PFA, permeabilized and stained for EdU and DNA. Zeiss Axio Observer was used to acquire pictures at 385 nm for nuclei stain and at 475 nm for EdU stain. The following settings were used: Intensity: 50 %, Exposure: 50 ms. The 10x objective was used and one 3x3 snap was taken in the middle of each well. In order to analyse proliferation, the "find maxima" tool in ImageJ (Schneider et al., 2012) was used to count EdU positive cells and total nuclei. The percentage of proliferating cells was calculated by dividing EdU positive cells by the total amount of cells.

2.13 Tube formation assay

The following list provides an overview of materials used. Disposables, pipettes etc. used are listed in 2.1.1.

- Apotome 3 (Carl Zeiss AG, Oberkochen, Germany)
- Axiocam 705 mono (Carl Zeiss AG, Oberkochen, Germany)

- Colibri 7 (Carl Zeiss AG, Oberkochen, Germany)
- Countess Automated Cell Counter (Invitrogen, Cat. No. C10227)
- ImageJ (Schneider et al., 2012)
- Matrigel® (Corning, Cat. No. 356234)
- Mikroskop Imager.M2m (Carl Zeiss AG, Oberkochen, Germany)
- PBS (Table 4)
- Trypan Blue Stain (Gibco, Cat. No. 15250)

In order to analyse compounds for angiogenic properties, a tube formation assay was performed using Matrigel®. 500.000 MuMECs were seeded in a 10 cm^2 TC dish and incubated for 24 hours (for details on muMEC cell culture see 2.1.3). Then, muMECs were washed with PBS and incubated for another 24 hours in starvation medium (Table 14). After, muMECs were detached from the culture dish using trypsin and counted using trypan blue and countess automated cell counter (for details see 2.1.2.2). Prior, in a 96 well plate 60 µl Matrigel® per well were added. The plate was then incubated for 30 minutes at 37 °C in order to let the Matrigel® solidify. Per well, 140 µl cell suspension containing 14.000 cells were added. Compounds of interest were added and the plate was incubated for 3 hours at 37 °C and 5 % CO_2. After incubation, one bright field picture in the middle of each well was acquired using the microscopy set up as listed above. The 5x objective was used to analyse the results. The total tube lengths per picture was measured using the straight line tool in ImageJ (Schneider et al., 2012).

2.14 Statistical analysis

GraphPad prism 6 software (GraphPad Software, Inc., California, USA) was used for statistical analysis. In order to compare two groups, two-tailed t-test (depending on the experimental design, paired or unpaired) was performed. For comparison of three or more groups, one-way ANOVA (again paired or unpaired) with Tukey's post hoc multiple

comparison test was applied. Resulting p-Values < 0.05 were considered significant. All results are shown as mean ± SEM.

3. Results

3.1 Role of NE on CXCL12-CXCR4-ACKR3-Axis in BA-muMEC crosstalk

As described in 1.4, preliminary experiments showed that cold exposure and thus sympathetic activation in BAT in mice, led to an upregulation of CXCL12 mRNA in BAT and BAT ECs. In order to investigate the effect of NE on murine BAs and muMECs further, a series of *in vitro* experiments was performed. CXCL12-CXCR4-ACKR3-axis mRNA expression levels were measured using RT-qPCR and the amount of CXCL12 released was determined using CXCL12 ELISA.

3.1.1 Role of NE on *Cxcl12-Cxcr4-Ackr3* expression and CXCL12 release in murine BAs

To mimic sympathetic activation in BAT, differentiated BAs were treated with 1 µM NE. After 24 hours of incubation, cells were harvested and mRNA expression of *Cxcl12*, *Cxcr4*, *Ackr3* as well as the amount of CXCL12 released was investigated (see 3.1). NE leads to an increase in oxygen consumption in BAs (Cannon and Nedergaard, 2004). Further, a regulatory role of HIF on CXCL12 during hypoxia has been shown (Vandyke et al., 2017). Different author's also suggested a possible correlation of HIF mRNA levels and HIF protein (Lin et al., 2022; Uchida et al., 2004). Thus, *Hif1α* and *Hif2α* mRNA expression levels were determined in order to examine whether HIF might potentially be upregulated and eventually interfere with regulation of CXCL12, CXCR4, and ACKR3 in BAs after NE treatment. As shown in Figure 4 (A-E), NE treatment led to significant upregulation of *Cxcl12*, *Ackr3* and *Hif2α* mRNA expression. Furthermore, BAs released ~89.5 % more CXCL12 into the supernatant after NE stimulus (Figure 4 F).

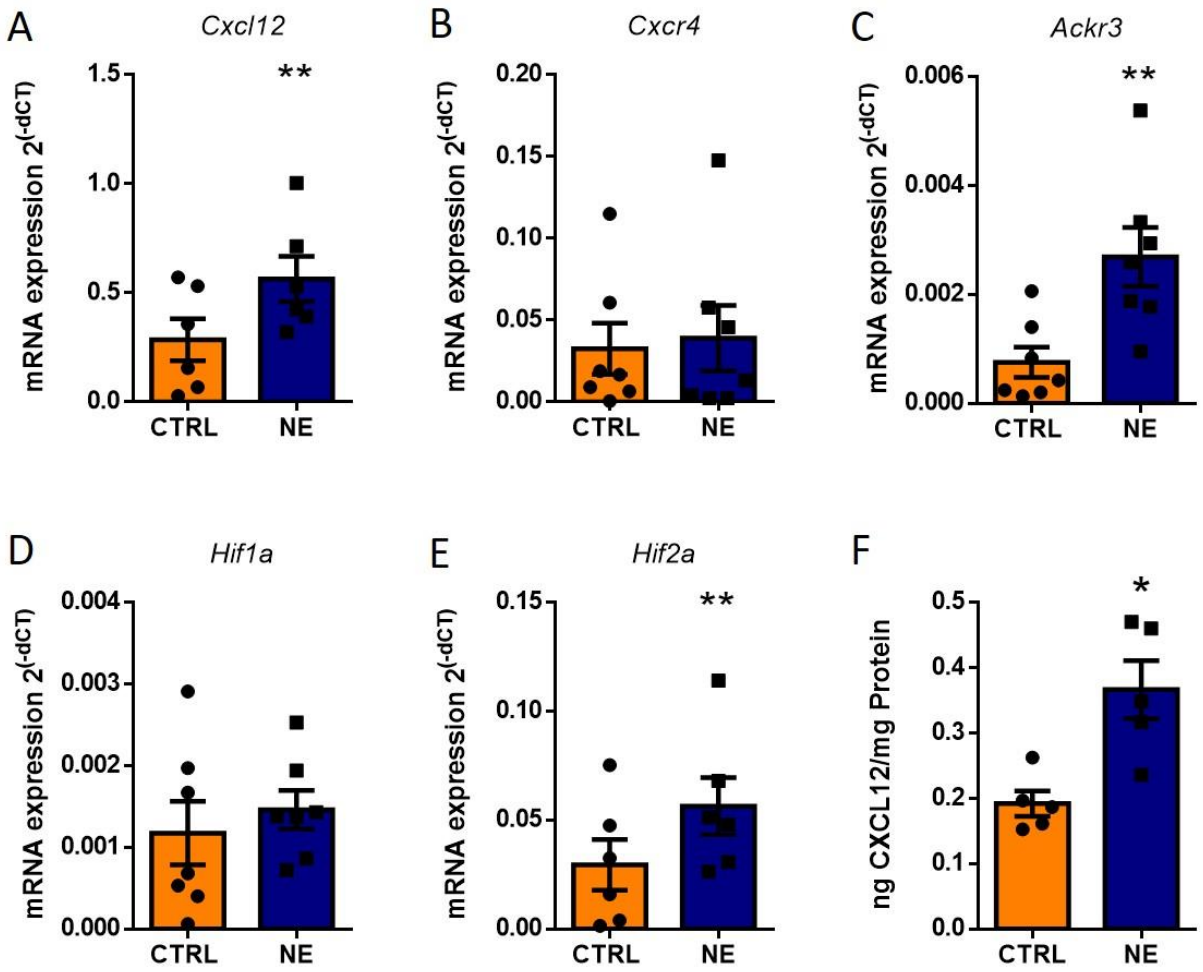

Figure 4 Effect of NE on CXCL12-CXCR4-ACKR3-axis in murine BAs

(A-E) Differentiated murine BAs were treated with 1 µM NE (dissolved in PBS) and incubated for 24 hours. Controls were treated with the corresponding volume of PBS. mRNA expression levels of (A) *Cxcl12*, (B) *Cxcr4*, (C) *Ackr3*, (D) *Hif1α*, and (E) *Hif2α* are shown (RT-qPCR). (F) shows the amount of CXCL12 released into the cell culture supernatant by BAs after 24 hours of treatment with 1 µM NE (ELISA). Gene expression levels were normalized to *Hprt* as an internal standard. Data are shown as mean ± SEM. t-test. n=5-7. **p*<0.05; ***p*<0.01.

3.1.2 Role of NE on *Cxcl12-Cxcr4-Ackr3* expression and CXCL12 release in muMECs

During BAT activation, not only BAs, but also every other cell type located in the tissue are potentially exposed to NE. Here, I focused on endothelial cells. Thus, it was asked whether sympathetic stimulation might also lead to a change in *Cxcl12*, *Cxcr4*, and *Ackr3* mRNA expression levels as well as CXCL12 released in muMECs. Further, *Hif1α* and *Hif2α* mRNA expression levels were determined. Therefore, muMECs were treated with

1 µM NE and incubated for 24 hours. The results are shown in Figure 5. NE did not have an effect on *Hif1α* and *Hif2α* mRNA expression levels (Figure 5 D-E). Furthermore, no significant change in mRNA expression levels of *Cxcl12*, *Cxcr4*, and *Ackr3* was observed (Figure 5 A-C). However, the relative amount of CXCL12 released into cell culture supernatant by muMECs showed an increase of ~36 % (means of controls and treated cells were 0.392 and 0.532 ng CXCL12/mg protein respectively, Figure 5 F).

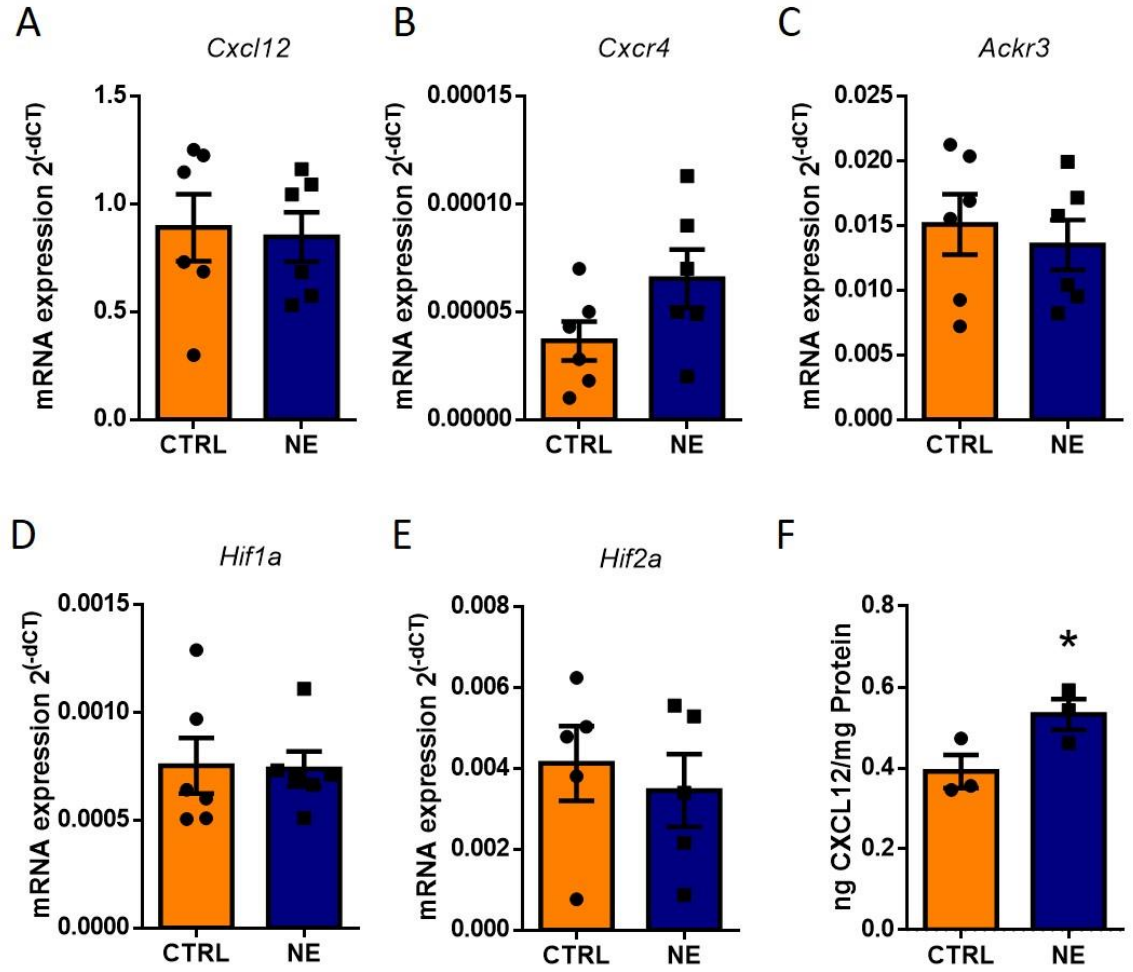

Figure 5 Effect of NE on CXCL12-CXCR4-ACKR3-axis in muMECs

MuMECs were treated with 1µM NE and incubated for 24 hours. Controls were treated with vehicle solution (PBS). mRNA expression levels of (A) *Cxcl12*, (B) *Cxcr4*, (C) *Ackr3*, (D) *Hif1a*, and (E) *Hif2a* are shown (RT-qPCR). (F) shows the amount of CXCL12 released by muMECs in cell culture supernatant per mg protein after NE treatment and incubation for 24 hours (ELISA). Gene expression levels were normalized to *Hprt* as an internal standard. Data are shown as mean ± SEM. t-test. N=3-6. *p<0.05

3.1.3 Role of NE on *Cxcl12-Cxcr4-Ackr3* expression in murine BA-muMEC co-culture

Next, the question whether muMECs might respond to NE when co-cultured with BAs was addressed. In order to do so, transwells containing muMECs were transferred to wells containing differentiated BAs. Once again, sympathetic stimulus was mimicked by treating both cell-types with 1 µM NE. After 24 hours of incubation, gene expression levels of *Cxcl12*, *Cxcr4*, *Ackr3*, and *Hif1α* as well as *Hif2α* were determined. Similar to the results shown in 3.1.1, mRNA levels of *Ackr3* and *Hif2α* were increased significantly in BAs (Figure 6 C, E). *Cxcl12* expression was also upregulated, albeit not statistically significant (Figure 6 A).

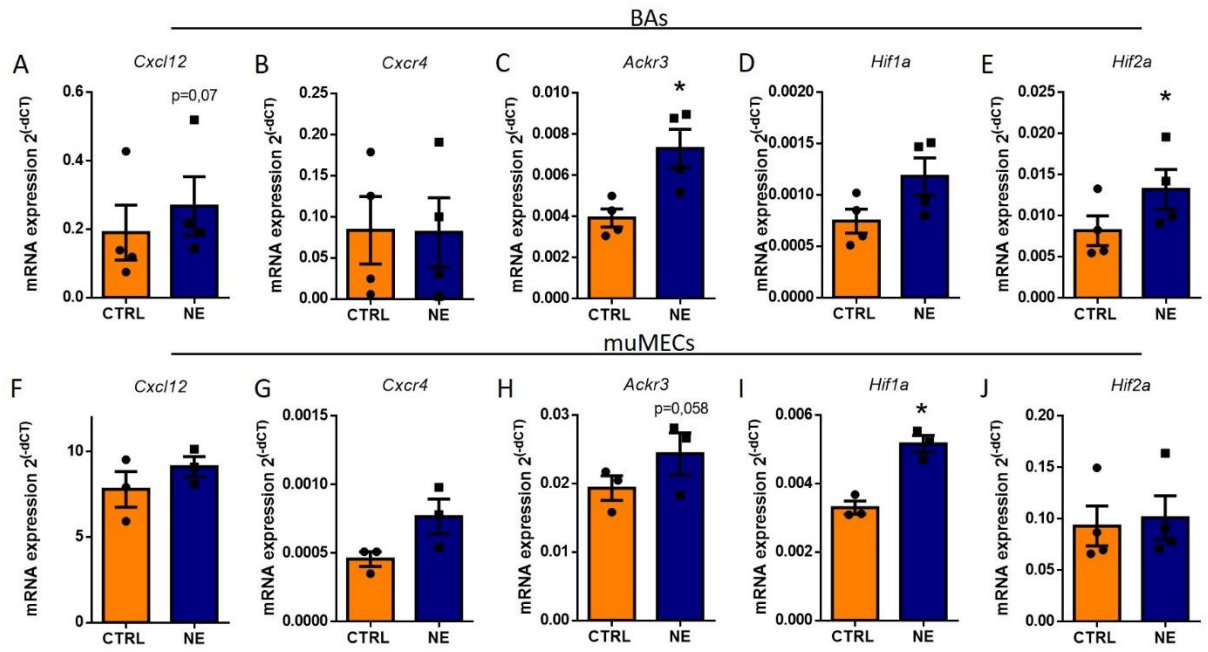

Figure 6 Effect of NE on CXCL12-CXCR4-ACKR3-axis in murine BA-muMEC co-culture

Inserts containing muMECs were co-cultured with BAs. The ratio of the surface of the culture vessel of BAs to muMECs was 3:1. The co-culture system was treated with 1 µM NE. (A-E) show *Cxcl12*, *Cxcr4*, *Ackr3*, *Hif1α*, and *Hif2α* mRNA expression levels in BAs. (F-J) show the respective mRNA expression levels in muMECs (RT-qPCR). Gene expression levels were normalized to Hprt as an internal standard. Data are shown as mean ± SEM. t-test. N=3-4. *p<0.05

In cocultured muMECs, the results differed from the muMECs cultured without BAs (shown in Figure 5). A significant upregulation of *Hif1α* was observed (Figure 6 I). Furthermore, mRNA expression levels of *Ackr3* showed a tendency for an increase (Figure 6 H).

Summarizing these results, NE leads to an increase in release of CXCL12 by BAs as well as muMECs. Furthermore, upon NE stimulus, mRNA expression levels of *Cxcl12*, *Ackr3*, and *Hif2α* are increased significantly in BAs. Meanwhile it seems, NE does not have an effect on expression patterns of the genes of interest in muMECs. However, in BA-muMEC co-culture, NE resulted in an increase of *Hif1α* mRNA expression and a strong tendency regarding expression levels of *Ackr3* in muMECs. Taken together, these findings suggest a potential regulatory role of HIF on CXCL12 and ACKR3 in BAs and muMECs. This corroborates our preliminary findings which suggested a regulatory role of hypoxia on CXCL12 in BAT. Thus, it was decided to investigate the role of hypoxia in this context further.

3.2 Role of hypoxia in CXCL12-CXCR4-ACKR3-axis in murine BA-muMEC crosstalk

During hypoxia, a regulatory role of HIF1α/HIF2α regarding CXCL12 expression has been reported in different types of cells (Kojima et al., 2011; Tabatabai et al., 2006; Vandyke et al., 2017). To examine the role of hypoxia in regulation of CXCL12, CXCR4, and ACKR3 in BAs, BAs were incubated under hypoxic conditions(1 % O_2) for 16, 24, or 48 hours respectively. Using RT-qPCR, gene expression levels of hypoxic cells were then compared to BAs incubated under normoxic conditions. Next to *Cxcl12*, *Cxcr4* and *Ackr3*, the gene expression levels for *Hif1α* and *Hif2α* were examined, in order to investigate which isoform has the leading function in BAs (Figure 7).

After 16 hours of hypoxia, an increase in mRNA expression of *Hif2α*, *Cxcl12*, *Cxcr4*, and *Ackr3* by 3.57-fold, 1.85-fold, 2.71-fold, and 5.88-fold respectively was observed (Figure 7 A-C, E). On the other hand, expression levels of *Hif1α* did not show a significant change (Figure 7 D). After 24 hours of hypoxia, the same gene expression patterns as for 16 hours of hypoxia were detected (Figure 7 F-J). A 4.23-fold increase in *Cxcr4* and a 4.61-fold increase in *Ackr3* expression was found to be statistically significant. Albeit not statistically significant, *Hif2α* and *Cxcl12* were also upregulated. After 48 hours of hypoxia, expression levels of *Cxcl12*, *Cxcr4*, *Ackr3*, and *Hif2α* were upregulated significantly (Figure 7 K-M, O).

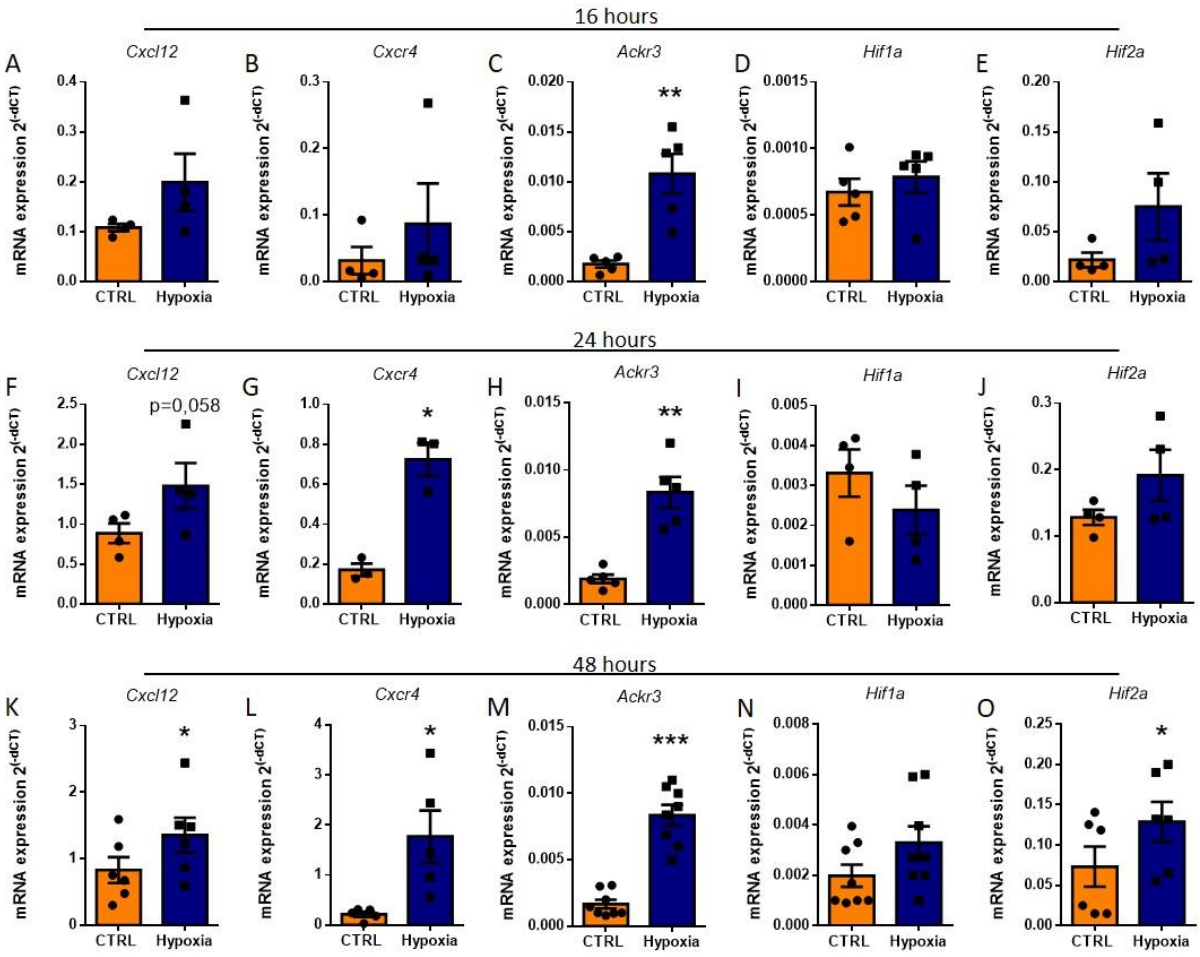

Figure 7 Role of hypoxia in gene expression levels of CXCL12-CXCR4-ACKR3-axis in murine BAs

Gene expression levels of *Cxcl12*, *Cxcr4*, *Ackr3*, *Hif1α*, and *Hif2α* in BAs after (A-E) 16 hours, (F-J) 24 hours and (K-O) 48 hours of incubation in hypoxia (1 % O_2) were determined and compared to gene expression levels of BAs grown in normoxia (RT-qPCR). Gene expression levels were normalized to *Hprt* as an internal standard. Data are shown as mean ± SEM. t-test. n=3-7. **p*<0.05; ***p*<0.01; ****p*<0.005.

In the following, a similar experiment was performed using muMECs. After incubation in hypoxia for 24 hours, a ~2-fold increase in *Cxcl12* mRNA expression was observed (Figure 8 A). After 48 hours of hypoxia, mRNA expression of *Ackr3* showed a ~4-fold upregulation (Figure 8 H). *Hif1α* and *Cxcl12* were upregulated significantly (Figure 8 F, I). Expression levels of *Hif2α* and *Cxcr4* did not change significantly (Figure 8 G, J).

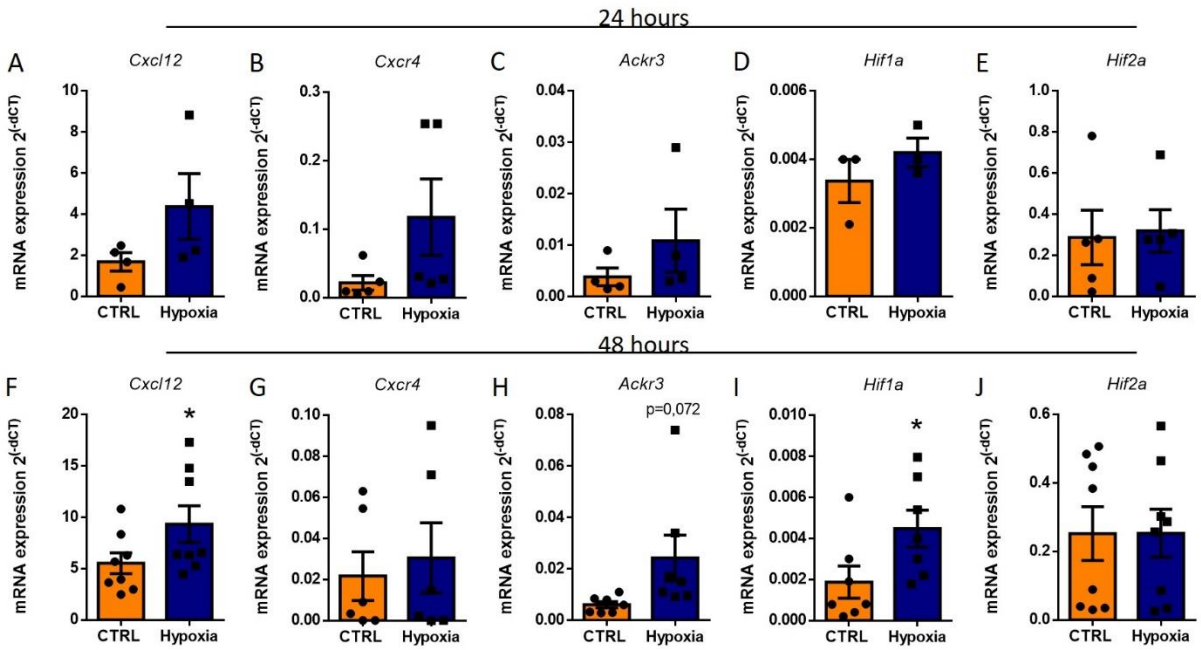

Figure 8 Role of hypoxia in gene expression levels of CXCL12-CXCR4-ACKR3-axis in muMECs

Gene expression levels of *Cxcl12*, *Cxcr4*, *Ackr3*, *Hif1α*, and *Hif2α* in muMECs were determined after (A-E) 24 and (F-J) 48 hours of incubation in hypoxia (1 % O_2) respectively (RT-qPCR). Controls were cultured in normoxia. Gene expression levels were normalized to *Hprt* as an internal standard. Data are shown as mean ± SEM. t-test. N=3-8. **p*<0.05.

Next, the question of whether hypoxia also leads to an increase in CXCL12 release in BAs and muMECs was addressed. For this, BAs and muMECs were incubated in hypoxic conditions. The cell culture supernatant was then harvested and the CXCL12 concentration was determined using ELISA. After 16 hours of hypoxia, CXCL12 released by BAs increased by ~40.5 % (Figure 9 A, mean value of normoxic and hypoxic cells were 0.145 ng/mg protein and 0.204 ng/mg protein respectively). In muMECs, a statistically significant increase of CXCL12 released was observed. After 48 hours of hypoxia, muMECs released 104 % more CXCL12 compared to controls incubated in normoxia.

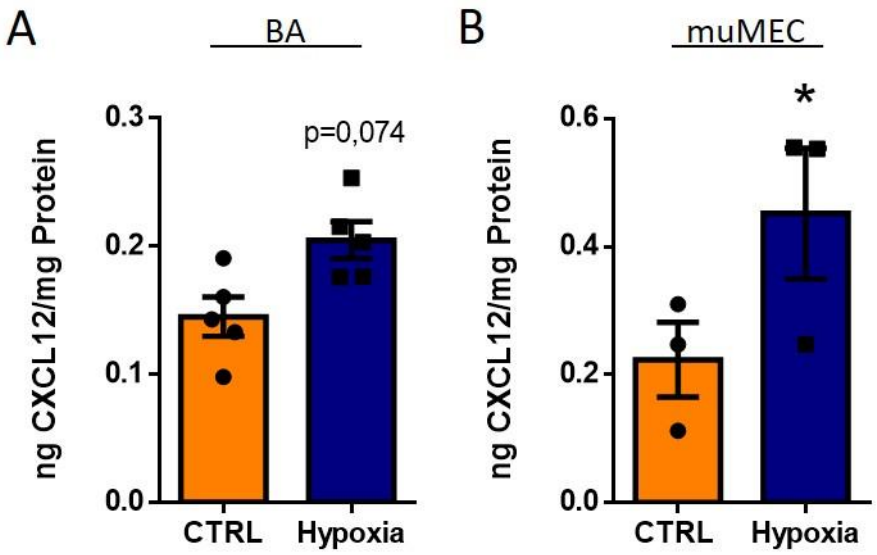

Figure 9 Hypoxia-mediated release of CXCL12 in murine BAs and muMECs

(A) BAs were incubated in hypoxia (1 % O_2) for 16 hours, (B) muMECs for 48 hours. The supernatant was harvested and CXCL12 concentration was determined (ELISA). CXCL12 concentrations were normalized to protein. For controls, BAs and muMECs were cultured in normoxic conditions respectively. Data are shown as mean ± SEM. t-test. (A) n=5; (B) n=3. *p<0.05.

These data reveal a regulatory role of hypoxia on CXCL12-CXCR4-ACKR3-axis in BAs and muMECs. Taken together, it appears that sympathetic stimulus and hypoxia might lead to increased levels of CXCL12 in BAT. However, knowledge of functional aspects of CXCL12 in BAT is limited. Thus, in order to tackle the hypothesis that CXCL12 might act in a paracrine or autocrine fashion in the crosstalk of BAs and MECs, different functional assays were performed next.

3.3 Effect of CXCL12 on murine BAs

3.3.1 Effect of CXCL12 on murine BA adipogenesis and thermogenesis

As described in 1.2.2, BAs have thermogenic and adipogenic properties. In order to examine whether CXCL12 has an influence on either property, BAs were differentiated and treated with 100 ng/ml CXCL12 in an acute and a chronic fashion. For acute treatment, differentiated BAs were incubated in the presence or absence CXCL12 for 24 hours. For a chronic exposure to CXCL12, BAs were differentiated as described in 2.1.2.3.: From D-2, 100 ng/ml CXCL12 were added to the culture medium each medium

change. BAs were exposed to CXCL12 for nine days in total. To study the effect of CXCL12 on BAs' adipogenic properties, gene expression levels of the adipogenic markers Elovl3 (Westerberg et al., 2006) and Fabp4 (Smathers and Petersen, 2011) were determined. Thermogenic properties were investigated using the classic BA defining thermogenic marker Ucp1. Further, in order to examine potential changes in fat droplet accumulation, chronically treated BAs were stained using Oil Red O.

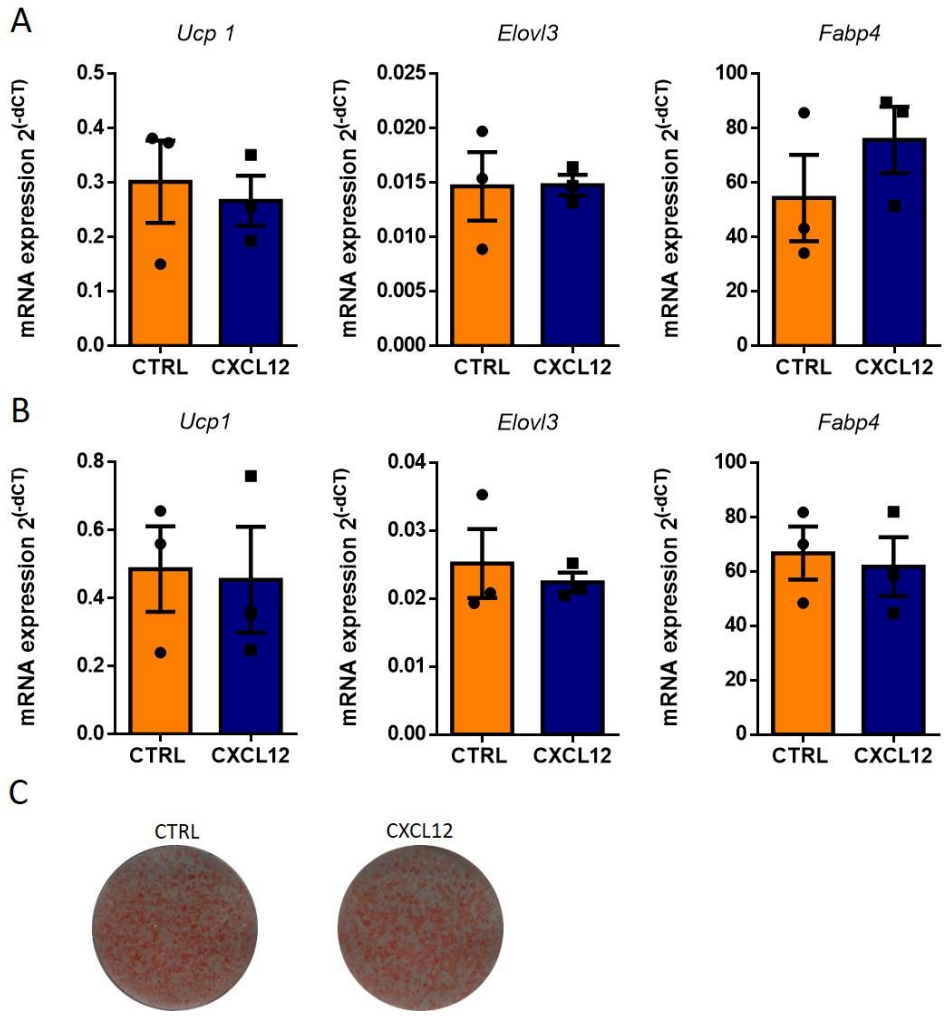

Figure 10 Effect of CXCL12 on adipogenic and thermogenic properties in murine BAs

(A) Differentiated BAs were treated with 100 ng/ml CXCL12. 24 hours after treatment, gene expression of adipogenic and thermogenic markers were determined (RT-qPCR). (B) Brown preadipocytes were treated chronically with 100 ng/ml CXCL12 during differentiation, gene expression of adipogenic and thermogenic markers were checked (RT-qPCR) and (C) Oil Red O staining was performed to demonstrate potential changes in lipid droplet accumulation (representative stainings shown). Gene expression levels were normalized to *Hprt* as an internal standard. Data are shown as mean ± SEM. t-test. n=3.

As shown in Figure 10 (A-B), no significant changes in mRNA expression levels of thermogenic and adipogenic markers for either treatment, acute or chronic, were observed. Additionally, Oil Red O staining did not show changes in lipid droplet accumulation (Figure 10 C).

3.3.2 Effect of CXCL12 on intracellular cAMP and lipolysis in murine BAs

Lipolysis is one of the main functions of BAs and is mediated by $G\alpha_s$ signalling and therefore (among others) controlled by the second messenger cAMP (Cannon and Nedergaard, 2004). In order to examine the role of CXCL12 in cAMP signaling in BAs, the intracellular concentration of cAMP as well as lipolysis after CXCL12 treatment was measured. ELISA was used to determine intracellular cAMP levels. Prior to CXCL12 treatment, BAs were incubated with IBMX (an unspecific phosphodiesterase [PDE] inhibitor) to inhibit cAMP degradation pathways (Sassone-Corsi, 2012). To investigate whether CXCL12 has an inhibiting or promoting effect on intracellular cAMP concentrations in BAs, BAs were treated with 100 ng/ml CXCL12, or 1 µM NE (as positive control) or a combination of 1 µM NE and 100 ng/ml CXCL12.

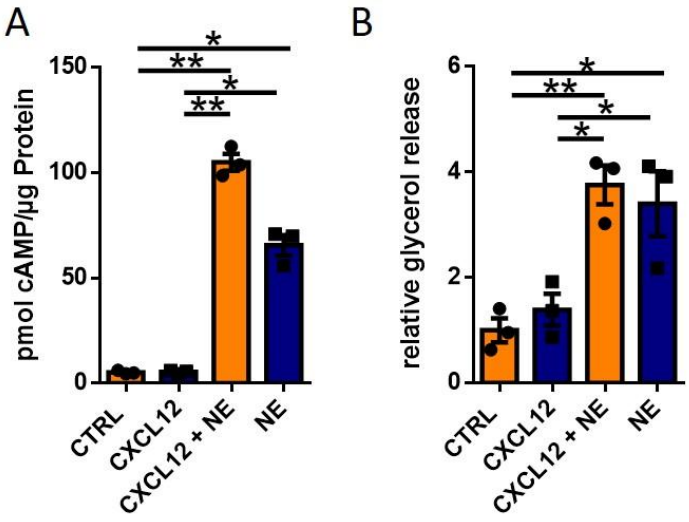

Figure 11 Influence of CXCL12 on intracellular cAMP and lipolysis in murine BAs

The effect of CXCL12 on (A) intracellular cAMP concentration (ELISA) and (B) lipolysis in non-activated and NE-stimulated BAs was investigated. 100 ng/ml CXCL12 and 1 µM NE were used respectively. Control was treated with vehicle solution (PBS), NE treatment was used as a high control. Prior to treatments, cAMP degradation pathways were pharmacologically inhibited for analysis of cAMP. Values were normalized to protein content. Data are shown as mean ± SEM. t-test. n=3. One-way ANOVA. *p<0.05; **p<0.01.

As shown in Figure 11 (A), CXCL12 did not have a significant effect on intracellular cAMP levels compared to the untreated control. NE led to a significant increase in intracellular cAMP compared to CTRL and CXCL12 (mean of control: 5.23 pmol/µg protein; mean of CXCL12 4.52 pmol/µg protein, mean of NE treated cells: 65.49 pmol/µg protein). In BAs treated with both, NE and CXCL12, intracellular cAMP concentrations were also increased compared to control and CXCL12. The combination of both drugs also showed an increase compared to NE alone (mean of NE: see above; mean of CXCL12 and NE: 104.94 pmol/µg protein). This change was not found to be statistical significant.

To stimulate lipolysis, BAs were also either treated with 100 ng/ml CXCL12, 1 µM NE, or a combination of 100 ng/ml CXCL12 and 1 µM NE. As displayed in Figure 11 (B) NE as well as the combination of NE and CXCL12 led to an upregulation of 339.99 % and 375.68 % in lipolysis, respectively, compared to untreated controls. An increase in lipolysis compared to CXCL12 treated cells was observed in cells treated with NE (increase of 271.73 %) or the combination of NE and CXCL12 (increase of 245.65 %).

Taken together, these findings suggest that CXCL12 does not have a major effect on differentiation and lipolysis and cAMP levels in BAs. However, CXCL12 might have a small additional effect on NE-induced effects.

3.4 Effect of CXCL12 in muMECs

3.4.1 Functional effect of CXCL12 in muMECs

To examine the functional aspects of CXCL12 in muMECs, different assays were performed. Using a Click-iT® EdU Alexa Fluor® 488 Imaging Kit, the influence of CXCL12 on muMEC proliferation was investigated. To do so, muMECs were treated with 100 ng/ml CXCL12 and incubated for eight hours. The ratio of cells replicating DNA – and thus preparing for mitosis – to all cells alive in the culture vessel was determined using microscopy. As shown in Figure 12 (C), a significant increase in proliferation after CXCL12 treatment was observed. In the control group, DNA replication was observed in 55.8 % of the cells within 8 hours of incubation. When treated with CXCL12, a mean value of 71.8 % of proliferating cells could be seen.

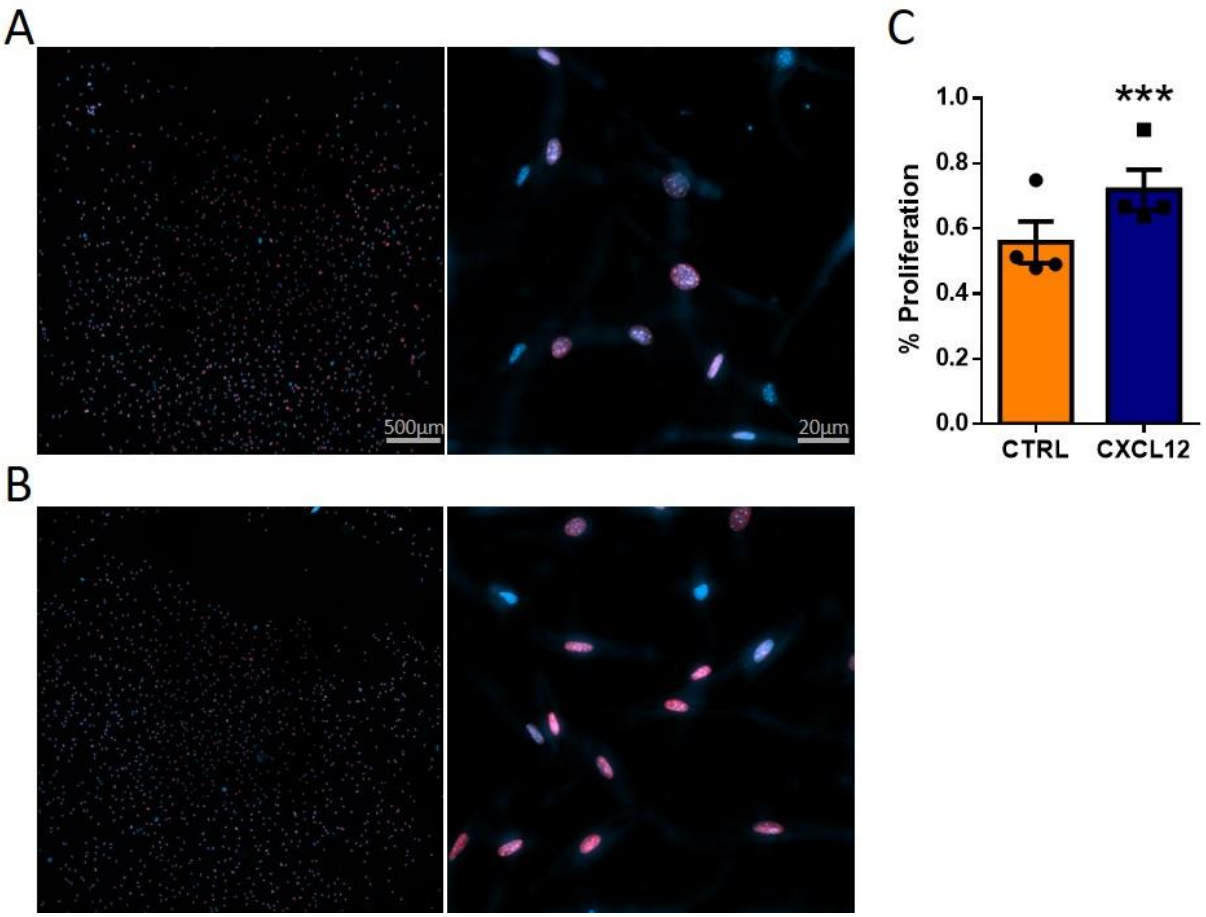

Figure 12 Effect of CXCL12 on proliferation in muMECs

MuMECs were (A) untreated or (B) treated with 100 ng/ml CXCL12 and incubated for 8 hours (representative pictures shown). Using Click-iT® EdU Alexa Fluor® 488 Imaging Kit, proliferating cells were detected. Total amount of cells was detected using Hoechst-nuclear stain. (C) For quantification, the ratio of proliferating cells to overall cells alive was determined. The resulting ratio was calculated to percentage of proliferating cells. Violet: EdU-positive cells. Blue: cell nuclei (Hoechst-nuclear stain). 10x (left) and 40x (right) objective was used respectively. Data are shown as mean ± SEM. t-test. (C) N=4. ****p*<0.005.

Next, the effect of CXCL12 on tube formation in muMECs was determined. To do so, muMECs were seeded on Matrigel®, treated with 100 ng/ml CXCL12 and incubated for 3 hours. In the following, pictures were acquired and the total length of the tube network was measured (Figure 13 C). The results showed a significant increase in total tube length of CXCL12-treated cells. Compared to control, the total length of the tube network in CXCL12-treated muMECs was increased by 33.21 %.

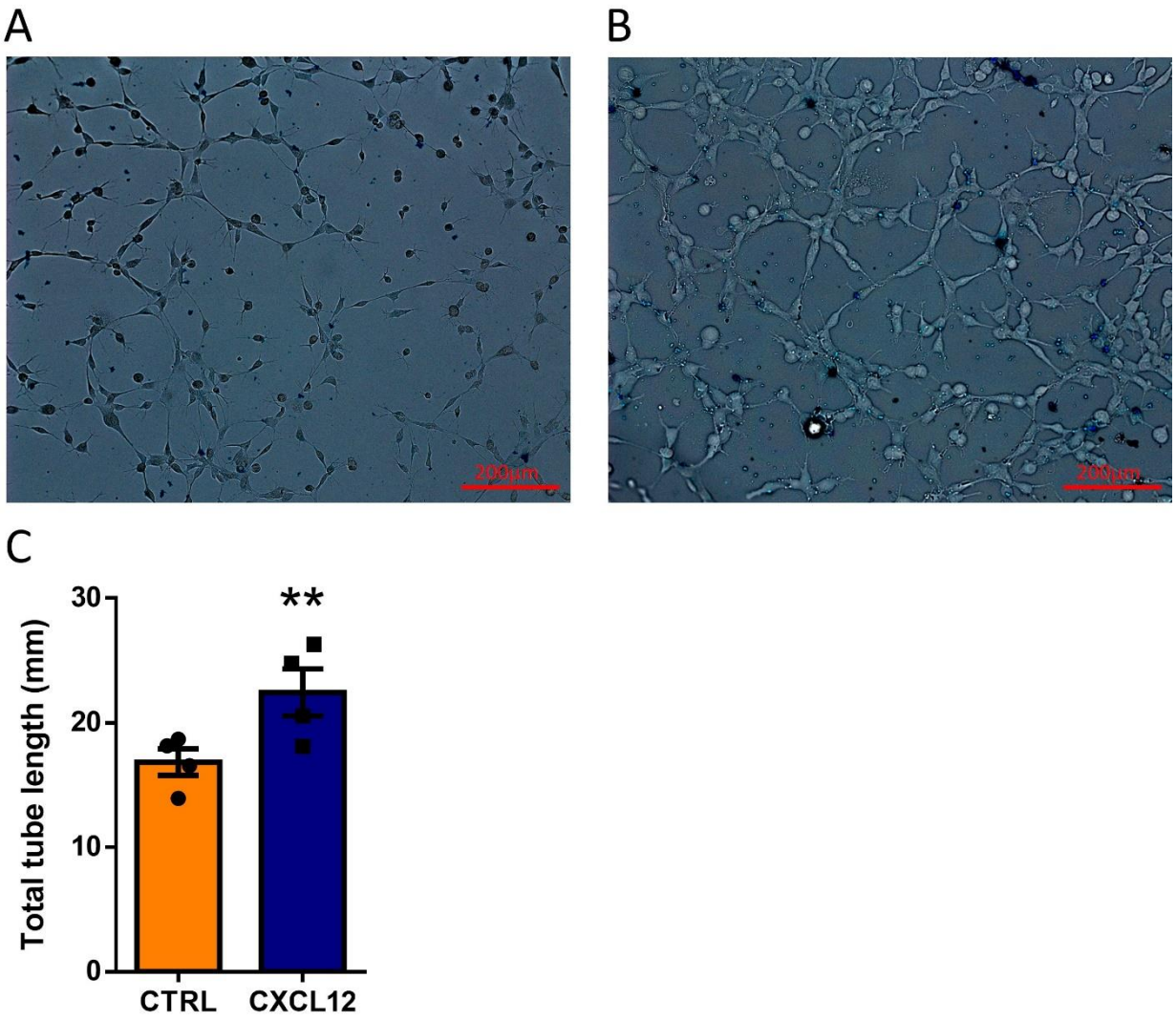

Figure 13 Tube formation in muMECs after CXCL12 treatment

MuMECs were seeded on Matrigel®, treated with 100 ng/ml CXCL12 and incubated for 3 hours. Representative pictures of (A) untreated control and (B) CXCL12-treated muMECs are shown (scale bar: 100 µm). For quantification, the total length of tubes formed was measured using ImageJ. Data are shown as mean ± SEM. t-test. (C) N=4. ***p*<0.01.

Furthermore, the effect of CXCL12 on cell migration in muMECs was investigated using a QCM™ 24-Well Colorimetric Cell Migration Assay: muMECs were allowed to migrate towards a concentration of 100 ng/ml CXCL12.The migrated cells were then stained, the stain was extracted and optical density was determined.

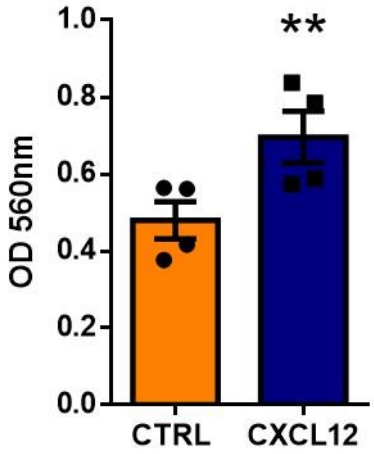

Figure 14 Effect of CXCL12 on migration in muMECs

muMECs were seeded in transwells with an 8 µm pore size polycarbonate membrane bottom. Transwells were then placed in medium containing 100 ng/ml CXCL12. After 8 hours of incubation, migrated cells were stained. After, the cells were washed and the staining solution was extracted from the stained cells. To identify the amount of cells migrated, the optical density of the extracted staining solution was measured at 560 nm. Data are shown as mean ± SEM. t-test. N=4. ***p*<0.01.

The results are shown in Figure 14. Optical density from cells migrating towards CXCL12 showed an increase of ~43 % compared to untreated controls.

3.4.2 CXCL12 signalling in muMECs

After examining the role of CXCL12 in a functional way in muMECs, the question came up, which receptors are involved. As described in 1.3.2, CXCL12 can potentially affect various intracellular pathways. Hence, it was decided to perform preliminary experiments focusing on CXCL12 signalling. To examine, which receptor mediates the functional aspects (as shown in 3.4.1), a Click-iT® EdU Alexa Fluor® 488 Imaging Kit was used to analyze proliferation. MuMECs were treated with CXCL12, plerixafor or a combination of both. As shown in Figure 15 (A), treatment with CXCL12 led to a relative increase of ~16.8 % on proliferation. On the other hand, when CXCR4 was inhibited, this effect of CXCL12 on proliferation did not occur (mean values for CTRL, CXCL12, plerixafor and CXCL12 + plerixafor were 59.33 %, 69.33 %, 53.01 %, and 51.92 % respectively).

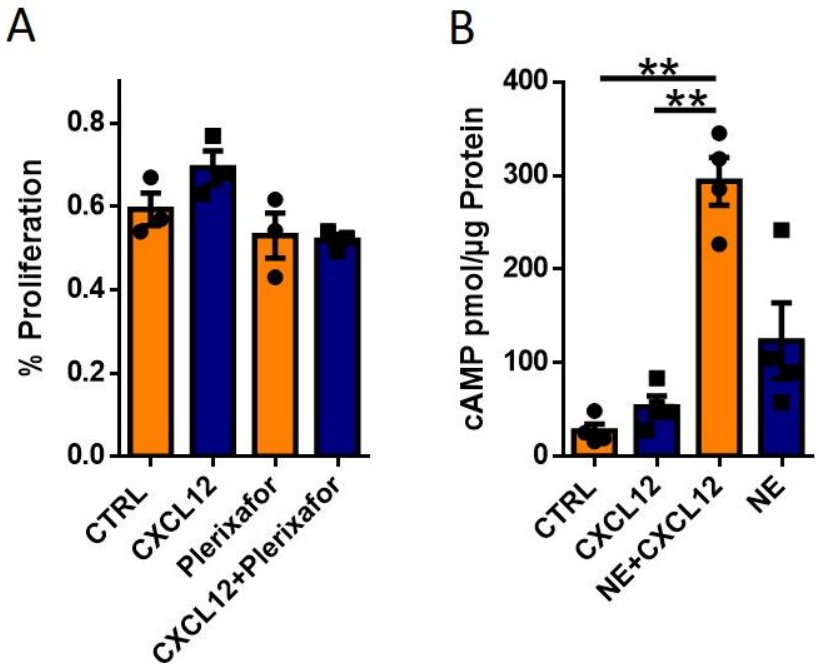

Figure 15 CXCL12 signalling in muMECs

(A) muMECs were treated with 100 ng/ml CXCL12, 10 µM plerixafor (specific CXCR4-inhibitor) or a combination of both. Proliferating cells were determined using Click-iT® EdU Alexa Fluor® 488 Imaging Kit. The ratio of proliferating cells to overall cells alive in the culture vessel was determined. (B) Intracellular cAMP concentrations after treatment with 100 ng/ml CXCL12, a combination of 1 µM NE + 100 ng/ml CXCL12 or 1 µM NE were determined using ELISA. Before cells were treated, PDEs were pharmacologically inhibited to block cAMP degradation using IBMX. Intracellular cAMP concentrations were normalized to protein content. Data are shown as mean ± SEM. One-way ANOVA. (A) N=3, (B) N=4. ***p*<0.01.

CXCL12 is signalling via cAMP (see 1.3.2). Since cAMP has been described to play a major role in cell proliferation (Stork and Schmitt, 2002), intracellular cAMP concentrations in muMECs were determined after treatment with 100 ng/ml CXCL12.

Figure 5 shows that muMECs release CXCL12 upon NE stimulus. NE is also known to stimulate $G\alpha_s$-signalling and thus lead to an increase in cAMP (Hanlon and Andrew, 2015). In order to investigate whether NE leads to a change in intracellular cAMP concentrations in muMECs – and whether CXCL12 might interfere with potential effects of NE – muMECs were also treated with 1 µM NE and a combination of 1 µM NE and 100 ng/ml CXCL12 respectively (Figure 15 B).

Treatment with CXCL12 led to a 1.95-fold change in intracellular cAMP compared to untreated control. NE increased intracellular cAMP levels by ~4.5-fold. Interestingly, the results showed a significant upregulation of ~ 10.85-fold when muMECs were treated with

a combination of NE + CXCL12. An increase of intracellular cAMP of cells treated with NE and CXCL12 compared to cells treated with CXCL12 was observed as well.

Summarizing these findings, it was shown that CXCL12 can increase proliferation, tube formation as well as migration in muMECs. Further, the data suggests that the functional aspects might be mediated via CXCR4 signalling.

3.5 Role of CXCL12 on murine BA-muMEC co-culture

After investigating the role of CXCL12 in BAs and muMECs in an isolated manner, the crosstalk of CXCL12 in BAs and muMECs was further explored by using a co-culture model. As described in 2.1.4.2, BAs and muMECs were co-cultivated and treated with 100 ng/ml CXCL12. After 48 hours of incubation, muMECs and BAs were stained using Hoechst-nuclear stain as well as Endomucin-stain. Total length of tubes formed by muMECs was then determined. In addition, RNA was isolated and mRNA expression levels of *Ucp1*, *Elovl3*, and *Fabp4* were determined in order to investigate whether CXCL12 has an effect on adipogenic or thermogenic properties in BAs in co-culture.

As shown in Figure 16 (C), a total increase in tube length of ~0.77 mm was observed. Gene expression levels of *Ucp1*, *Elovl3*, and *Fabp4* did not show significant changes (Figure 16 D).

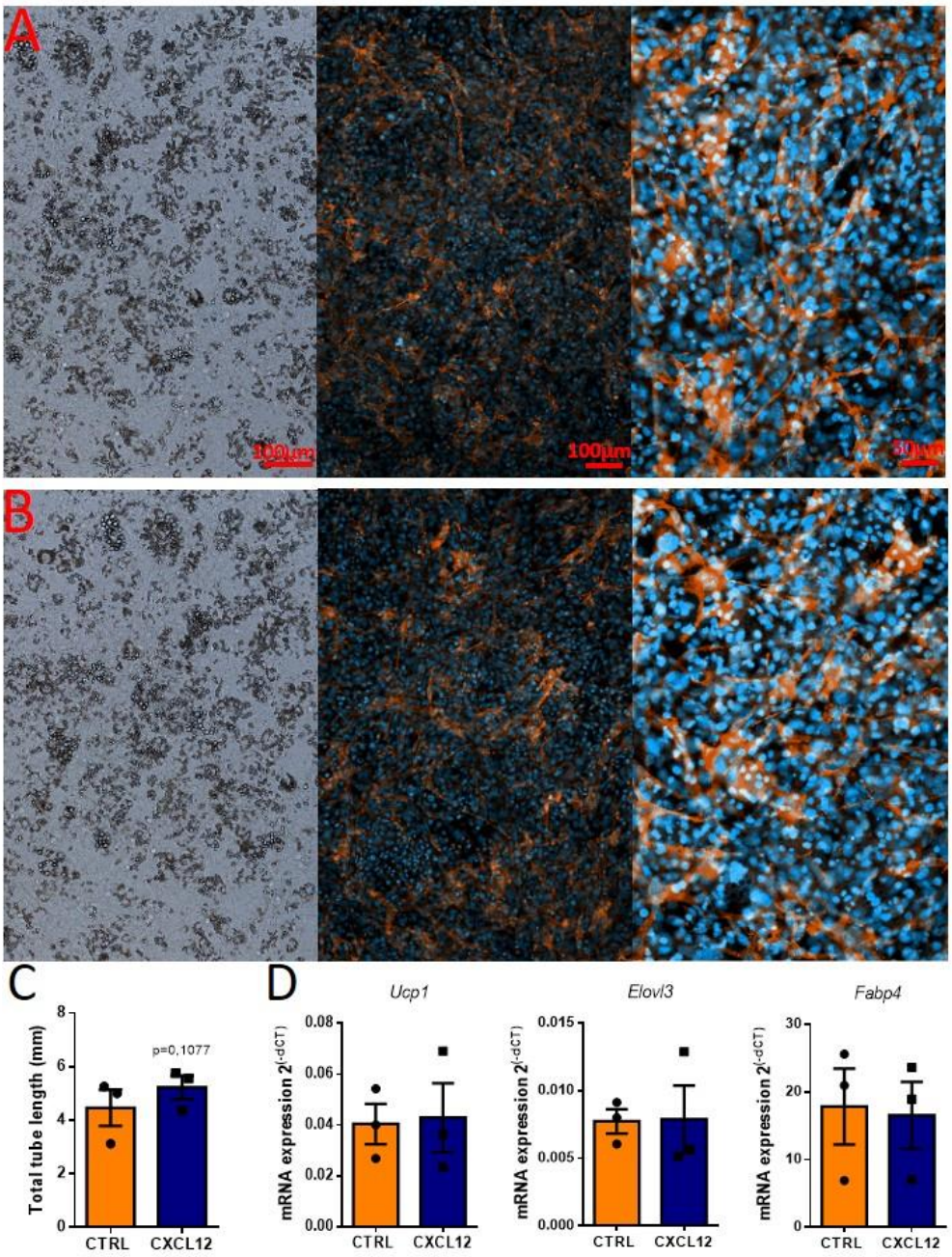

Figure 16 Effect of CXCL12 on co-culture of murine BAs and muMECs

BAs were co-cultivated with muMECs and treated with 100 ng/ml CXCL12. After 48 hours of incubation, cells were either (A-B) fixed and stained, or (D) RNA was isolated. Representative pictures of (A) untreated control and (B) CXCL12 treated cells are shown. Left pictures show a brightfield image. Middle and right are stained for nuclei (Hoechst-nuclear stain) and Endomucin. Nuclei of all cells are displayed in blue, muMECs are shown in orange. (C) Total length of tubes formed by muMECs in the co-culture system was determined using ImageJ. (D) Gene expression levels of *Ucp1*, *Elovl3*, and *Fabp4* were determined (RT-qPCR). Gene expression levels were normalized to *Hprt* as an internal standard. Data are shown as mean ± SEM. t-test. (C,D) n=3. $p<0.05$ was considered to be significant.

In summary, while a tendency in increasing total length of the tube network formed by muMECs was observed when treated with CXCL12 in the presence of BAs. My data suggest that BAs were not affected by the CXCL12 treatment.

4. Discussion

4.1 Role of NE and hypoxia on CXCL12 in murine BAs and muMECs

Upon cold exposure, BAT is activated via NE released by the SNS (Cannon and Nedergaard, 2004). Thus, next to BAs, other cells located in the tissue are possibly exposed to NE during BAT activation as well.

As shown here, *in vitro* mimicry of sympathetic activation using 1 µM NE led to an increase in mRNA expression levels of *Cxcl12*, *Ackr3*, and *Hif2α* in BAs. Furthermore, upon NE treatment CXCL12 secreted by BAs increased significantly. It is known that NE leads to an increase in oxygen consumption in BAT (Cannon and Nedergaard, 2004). However, it appears NE activation might not just increase oxygen consumption, but even induce hypoxia in BAs. A regulatory role of hypoxia regarding CXCL12 expression has been described in a variety of different cells such as haematopoietic progenitor cells and multiple myeloma plasma cells, however not in BAs (Tabatabai et al., 2006; Vandyke et al., 2017). It has also been reported, that HIF2α mRNA and protein can be upregulated upon hypoxia in lung epithelial cells (Uchida et al., 2004). Taken together, these findings suggest that NE might regulate CXCL12 and ACKR3 in BAs via an increase in oxygen consumption and thus potentially via HIF2α.

In muMECs, an increase of CXCL12 in the cell culture supernatant was detected after NE treatment. It appears, NE stimulus directly leads to muMECs secreting CXCL12. Importantly, CXCL12 is known to be a homeostatic chemokine (Zlotnik und Yoshie, 2000). For future aspects, a detailed study of whether muMECs might potentially synthesize CXCL12 continuously or even obtain depots of intracellular CXCL12 which are released upon sympathetic stimulus, might reveal interesting novel findings to this context.

Intriguingly, when cultured in hypoxia (1 % O_2), an upregulation of mRNA expression levels of *Cxcl12*, *Cxcr4*, and *Ackr3* was observed in BAs. In muMECs on the other hand, it seems that *Cxcl12* and *Ackr3* are also regulated by hypoxia, but not *Cxcr4*. Further, an upregulation of *Hif2α* and *Hif1α* in BAs and muMECs respectively was observed. Upregulation of mRNA expression levels of the different HIF-isoforms in BAs and muMECs, hint towards the idea of HIF1α being the predominant isoform in muMECs and

HIF2α in BAs respectively. ELISA showed that not just mRNA expression levels, but also the amount of CXCL12 released by either cell type was increased after incubation in hypoxic conditions. In conclusion, these data suggest a direct regulatory role of hypoxia regarding CXCL12-CXCR4-ACKR3-axis in BAs and muMECs.

Taken together, these findings imply that upon BAT activation, CXCL12 release is stimulated. Potentially, the effect of NE and hypoxia might even act in a synergistic fashion, leading to a rapidly increasing concentration of CXCL12 in the tissue. Importantly, the regulatory role of NE and hypoxia regarding CXCL12 in muMECs and BAs adds up to the findings presented by different researchers in the literature. It has been shown that hypoxia leads to upregulation of CXCL12 in umbilical vascular endothelial cells (Sun et al., 2019). Further, it has been described that NE stimulus can lead to an increase in CXCL12 secretion in vascular endothelial cells (Wu et al., 2016). However, unlike shown in this study, it has also been shown that hypoxia can potentially lead to upregulation of CXCR4 in endothelial progenitor cells (Tu et al., 2016). The regulatory role of NE and hypoxia regarding CXCL12 in BAs specifically has not been addressed in literature before.

Thus, a comparison of activated BAT to the microenvironment in different cancers could be drawn. In tumor microenvironment, cancer cells can proliferate rapidly which can lead to hypoxia (Jing et al., 2019). To tackle hypoxia, a greater supply of oxygen is needed. This can be accomplished by an increase in neoangiogenesis. It has been shown that increased levels of CXCL12 support the process of neoangiogenesis in cancer (Kryczek et al., 2005). Similar to the tumor microenvironment, high amounts of oxygen are required for BAT function (Cannon and Nedergaard, 2004). As shown here, activation of BAT might potentially even lead to hypoxia. Thus, the increase of CXCL12 released might also play a role in neoangiogenesis in BAT and therefore be an important factor for maintaining sufficient oxygen supply and – finally – function of BAT.

Importantly, the findings presented here are limited by different factors. While ELISA was used to show an increase in CXCL12 in cell culture supernatant, data regarding expression levels of receptors were acquired using RT-qPCR. Potentially, mRNA might be degraded and thus the actual increase in protein synthesized might differ from the changes seen on mRNA level. Furthermore, HIF1α and HIF2α are subject to a special

regulatory pathway. Both proteins are synthesized and degraded constantly. Upon hypoxia, the degradation pathway is inhibited and functional protein can accumulate (Yee Koh et al., 2008). However, in different HIF-isoforms, it has been shown that mRNA and protein can show a corresponding increase upon hypoxic state (Lin et al., 2022; Uchida et al., 2004). Further, it is well known that HIF protein accumulates upon absence of sufficient O_2 supply. mRNA data presented in this study shows an increase in HIF1α/HIF2α mRNA respectively when cells were exposed to hypoxia. Taken together, the increased gene expression levels of HIF1α/HIF2α hint towards a regulatory role regarding CXCL12-CXCR4-ACKR3-axis in the crosstalk of BAs and MECs. Yet again, as described above, the findings made on mRNA level need to be interpreted in a critical fashion and further protein analysis are required to verify these data.

Moreover, a detailed analysis of intracellular pathways stimulated by either NE or hypoxia, which leads to release of CXCL12 in BAs and muMECs, is required for detailed understanding of CXCL12 physiology in either cell type. Additionally, besides endothelial cells and adipocytes, other types of cells such as immune cells, fibroblasts, and neurons are located in BAT (Rosen and Spiegelman, 2014). These types of cells potentially also interfere with CXCL12 signalling in BAT. Recruitment of macrophages in adipose tissue mediated by CXCL12 has been described before (Kim et al., 2014). Thus, investigation of CXCL12 in crosstalk of adipocytes and other resident cell types might also bring new insights into BAT biology. Furthermore, *in vivo* experiments need to be performed to verify these *in vitro* findings and to study potential effects of CXCL12 released by BAT on whole body metabolism.

4.2 Functional aspects of CXCL12 in murine BAs and muMECs

After establishing that CXCL12 is released and CXCL12 as well as its receptors are upregulated upon specific stimuli in BAs and muMECs, an investigation of CXCL12 function on either cell type followed.

As shown here, neither acute, nor chronical treatment of BAs with 100 ng/ml CXCL12 led to significant changes in thermogenic and adipogenic markers. It appears, CXCL12 does not interfere with important transcriptional pathways and major transcriptional factors such as PPARγ and PRDM16 which are key regulators of adipogenesis and thermogenesis

(Rosen and MacDougald, 2006; Seale et al., 2007). These findings are further supported by the fact that Oil Red O stainings of differentiated adipocytes after chronical treatment with CXCL12 did not show major changes in lipid droplet accumulation, suggesting once again that exposure to CXCL12 does not have a significant effect on adipocyte biology.

For further examination, lipolysis assay was performed and concentrations of the second messenger cAMP – which is a key mediator of sympathetic activation in BAs (Cannon and Nedergaard, 2004) – were investigated. Once again, CXCL12 did not have a significant effect on either process. Intriguingly, upon stimulation with a combination of CXCL12 and NE, the increase in intracellular cAMP was even greater than the increase seen in cells solely treated with NE. As described in 1.3.2, CXCL12 is known to influence a variety of intracellular pathways. For example, it can inhibit ACs (and thus inhibit cAMP production), but also increase intracellular calcium (Janssens et al., 2018). Importantly, it has been reported that calcium can also interfere with ACs – in an inhibitory as well as a stimulating fashion (Cooper et al., 1995). Thus, the greater increase of cAMP levels in cells treated with NE and CXCL12 might possibly be explained by a synergistic effect of NE and eventually rising levels of intracellular calcium. These findings hint towards a potential alteration of NE pathing in BAs mediated by CXCL12 in an autocrine or paracrine fashion.

CXCL12 has been described to function as a homeostatic chemokine (Zlotnik and Yoshie, 2000). Taken together, the data presented here suggest that CXCL12 does not interfere with basal BA development or function. Meanwhile, CXCL12 and its receptors are expressed in BAs and even upregulated upon specific stimuli (NE treatment upregulates CXCL12 and ACKR3 mRNA expression levels, while hypoxia increases CXCL12, CXCR4, and ACKR3 mRNA expression levels). Additionally, it has been shown that CXCR4 deficiency in BAT in mice can influence the response to insulin (Kurita et al., 2019). Adipose tissue specific deficiency of CXCR4 has also been shown to alter adipocyte function. As Yao and colleagues presented, deficiency of CXCR4 in adipose tissue in mice being fed a high fat diet, led to an exacerbation of obesity (Yao et al., 2014). In contrast to the data presented here, Kurita et al. showed an increase in UCP1 expression in BAs as well as an increase in BA activity after BAs were treated with CXCL12 (Kurita et al., 2019). This contradiction might be due to the fact that cell culture methods and

concentrations of CXCL12 used differed from one another in the study presented here and the study described above.

As presented in this thesis, an increase in proliferation, migration as well as tube formation was observed after treatment with CXCL12 in muMECs. Proliferation, migration and tube formation are mechanisms which promote angiogenesis (Carmeliet and Jain, 2011). Hypoxia is a classic stimulus leading to an increase in blood vessel formation (Fong, 2008). Taken the regulative aspects of hypoxia regarding CXCL12 and the functional aspects described above together, it seems CXCL12 enhances neoangiogenesis. The data also suggest that the effect of CXCL12 might be mediated by CXCR4.

Using a direct co-culture model, similar findings to the respective mono-culture models were made. In co-culture of BAs and muMECs, CXCL12 treatment did not have an effect on thermogenic or adipogenic markers in BAs. In muMECs on the other hand, a tendency towards an increase in total tube length was observed. This supports the idea of CXCL12 functioning as a homeostatic chemokine in BAT, primarily influencing angiogenesis and supply of oxygen in the tissue.

In tumor microenvironment, CXCL12 has been shown to play a role in angiogenesis (Kryczek et al., 2005). Further, using different kinds of endothelial cells, a pro-angiogenic effect of CXCL12 was reported by different researchers, analysing *in vitro* and *in vivo* models (Mirshahi et al., 2000; Zhang et al., 2017; Ziegler et al., 2016).

Even though these findings propose that CXCL12 plays a role in angiogenesis in BAT, my study is limited by the fact that mainly *in vitro* models using muMECs and BAs to mimic BAT microenvironment were used. BAT specific ECs could potentially respond in a different way than muMECs to CXCL12 stimulus. Further, CXCL12 being a homeostatic chemokine, BAT and BA specific knock out models are needed to verify the findings proposed here and to generate further insight into the function of CXCL12 in BAT. Since BAs and muMECs release CXCL12 upon NE stimulus, performing a detailed investigation of the role of CXCL12 in activated BAT would surely also add interesting findings to the growing body of BAT literature.

In conclusion, on the hunt for novel strategies to sustain BAT activity and function, it appears, CXCL12 might be a promising candidate to supply sufficient oxygen to active BAT. In this work, a novel crosstalk of BAs and muMECs communicating via CXCL12 was identified which potentially even mediates neoangiogenesis in BAT, adding another piece to the unsolved puzzle of BAT biology.

5. Summary

Obesity is caused by an imbalance of energy intake and energy expenditure and is a major risk factor for different diseases such as type II diabetes mellitus. In the past decades, the prevalence of obesity has been increasing rapidly.

To date, few treatment options which differ from lifestyle changes are known. On the hunt for a new approach to treat obesity, brown adipose tissue (BAT) was re-discovered in humans less than two decades ago. Mediated by its unique protein UCP1, BAT's main function consists of non-shivering thermogenesis, a process which is mediated by cold and the sympathetic nervous system and allows BAT to burn through immense amounts of energy. However, clinical trials focussing BAT as a pharmacological target to increase energy expenditure have failed so far. Among others, this is due to the fact that today's understanding of BAT biology still is quite limited.

CXCL12 is a homeostatic chemokine which is known to function in a variety of important physiological processes such as angiogenesis, cardiogenesis and so forth. Its function is mediated by two different receptors: CXCR4 and ACKR3. Late published data suggested, CXCL12 plays an important role in BAT homeostasis and might even be able to activate BAT.

Since BAT's function is highly dependent on sufficient O_2 supply and muMECs are required for neoangiogenesis to occur, this work focussed on investigating the role of CXCL12 in a potential crosstalk of BAs and muMECs.

Performing *in vitro* experiments, this work showed that upon NE stimulus, BAs and muMECs release increased amounts of CXCL12. By exposing both cell types to hypoxia, it was shown that hypoxia also leads to an increase in CXCL12 released from both cells. Further, the data showed an increase of expression of *Cxcl12*, *Cxcr4*, and *Ackr3* mRNA in BAs and an increase of *Cxcl12* and *Ackr3* mRNA in muMECs after hypoxia.

In the following, the functional effect of CXCL12 on BAs and muMECs was investigated. The results showed that CXCL12 does not seem to have an impact on BA differentiation or basal function. In muMECs on the other hand, an increase in proliferation, tube formation and migration after CXCL12 treatment was seen, suggesting an important role

of CXCL12 in neoangiogenesis in BAT. Further experiments suggested the functional aspects might be mediated via CXCR4 signalling.

Finally, a co-culture model was used to examine potential direct interactions of BAs and muMECs via CXCL12. Adding up to the experiments performed in mono-culture, after CXCL12 treatment no differences in BAs were seen, but an increase in tube formation was observed.

In summary, in this thesis, a novel crosstalk, which potentially plays a major role in neoangiogenesis in BAT, of BAs and muMECs interacting via CXCL12 signalling was identified.

6. List of figures

7. List of tables

8. References

Afshin A, Forouzanfar MH, Reitsma MB, Sur P, Estep K, Lee A, Marczak L, Mokdad AH, Moradi-Lakeh M, Naghavi M, Salama JS, Vos T, Abate KH, Abbafati C, Ahmed MB, Al-Aly Z, Alkerwi A, Al-Raddadi R, Amare AT, Amberbir A, Amegah AK, Amini E, Amrock SM, Anjana RM, Ärnlöv J, Asayesh H, Banerjee A, Barac A, Baye E, Bennett DA, Beyene AS, Biadgilign S, Biryukov S, Bjertness E, Boneya DJ, Campos-Nonato I, Carrero JJ, Cecilio P, Cercy K, Ciobanu LG, Cornaby L, Damtew SA, Dandona L, Dandona R, Dharmaratne SD, Duncan BB, Eshrati B, Esteghamati A, Feigin VL, Fernandes JC, Fürst T, Gebrehiwot TT, Gold A, Gona PN, Goto A, Habtewold TD, Hadush KT, Hafezi-Nejad N, Hay SI, Horino M, Islami F, Kamal R, Kasaeian A, Katikireddi SV, Kengne AP, Kesavachandran CN, Khader YS, Khang Y-H, Khubchandani J, Kim D, Kim YJ, Kinfu Y, Kosen S, Ku T, Defo BK, Kumar GA, Larson HJ, Leinsalu M, Liang X, Lim SS, Liu P, Lopez AD, Lozano R, Majeed A, Malekzadeh R, Malta DC, Mazidi M, McAlinden C, McGarvey ST, Mengistu DT, Mensah GA, Mensink GBM, Mezgebe HB, Mirrakhimov EM, Mueller UO, Noubiap JJ, Obermeyer CM, Ogbo FA, Owolabi MO, Patton GC, Pourmalek F, Qorbani M, Rafay A, Rai RK, Ranabhat CL, Reinig N, Safiri S, Salomon JA, Sanabria JR, Santos IS, Sartorius B, Sawhney M, Schmidhuber J, Schutte AE, Schmidt MI, Sepanlou SG, Shamsizadeh M, Sheikhbahaei S, Shin M-J, Shiri R, Shiue I, Roba HS, Silva DAS, Silverberg JI, Singh JA, Stranges S, Swaminathan S, Tabarés-Seisdedos R, Tadese F, Tedla BA, Tegegne BS, Terkawi AS, Thakur JS, Tonelli M, Topor-Madry R, Tyrovolas S, Ukwaja KN, Uthman OA, Vaezghasemi M, Vasankari T, Vlassov VV, Vollset SE, Weiderpass E, Werdecker A, Wesana J, Westerman R, Yano Y, Yonemoto N, Yonga G, Zaidi Z, Zenebe ZM, Zipkin B, Murray CJL. Health Effects of Overweight and Obesity in 195 Countries over 25 Years. The New England journal of medicine 2017; 377: 13–27

Atit R, Sgaier SK, Mohamed OA, Taketo MM, Dufort D, Joyner AL, Niswander L, Conlon RA. Beta-catenin activation is necessary and sufficient to specify the dorsal dermal fate in the mouse. Developmental biology 2006; 296: 164–176

Bachelerie F, Ben-Baruch A, Burkhardt AM, Combadiere C, Farber JM, Graham GJ, Horuk R, Sparre-Ulrich AH, Locati M, Luster AD, Mantovani A, Matsushima K, Murphy PM, Nibbs R, Nomiyama H, Power CA, Proudfoot AEI, Rosenkilde MM, Rot A, Sozzani S,

Thelen M, Yoshie O, Zlotnik A. International Union of Basic and Clinical Pharmacology. corrected. LXXXIX. Update on the extended family of chemokine receptors and introducing a new nomenclature for atypical chemokine receptors. Pharmacological reviews 2014; 66: 1–79

Balabanian K, Lagane B, Infantino S, Chow KYC, Harriague J, Moepps B, Arenzana-Seisdedos F, Thelen M, Bachelerie F. The chemokine SDF-1/CXCL12 binds to and signals through the orphan receptor RDC1 in T lymphocytes. The Journal of biological chemistry 2005; 280: 35760–35766

Barbieri F, Bajetto A, Stumm R, Pattarozzi A, Porcile C, Zona G, Dorcaratto A, Ravetti J-L, Minuto F, Spaziante R, Schettini G, Ferone D, Florio T. Overexpression of stromal cell-derived factor 1 and its receptor CXCR4 induces autocrine/paracrine cell proliferation in human pituitary adenomas. Clinical cancer research : an official journal of the American Association for Cancer Research 2008; 14: 5022–5032

Bartelt A, Bruns OT, Reimer R, Hohenberg H, Ittrich H, Peldschus K, Kaul MG, Tromsdorf UI, Weller H, Waurisch C, Eychmüller A, Gordts PLSM, Rinninger F, Bruegelmann K, Freund B, Nielsen P, Merkel M, Heeren J. Brown adipose tissue activity controls triglyceride clearance. Nat Med 2011; 17: 200–205

Becher T, Palanisamy S, Kramer DJ, Eljalby M, Marx SJ, Wibmer AG, Butler SD, Jiang CS, Vaughan R, Schöder H, Mark A, Cohen P. Brown adipose tissue is associated with cardiometabolic health. Nat Med 2021; 27: 58–65

Benaiges D, Goday A, Pedro-Botet J, Más A, Chillarón JJ, Flores-Le Roux JA. Bariatric surgery: to whom and when? Minerva endocrinologica 2015; 40: 119–128

Braissant O, Wahli W. Differential expression of peroxisome proliferator-activated receptor-alpha, -beta, and -gamma during rat embryonic development. Endocrinology 1998; 139: 2748–2754

Buemann B, Toubro S, Astrup A. Effects of the two beta3-agonists, ZD7114 and ZD2079 on 24 hour energy expenditure and respiratory quotient in obese subjects. International

journal of obesity and related metabolic disorders : journal of the International Association for the Study of Obesity 2000; 24: 1553–1560

Cahill GF. Starvation in man. Clinics in Endocrinology and Metabolism 1976; 5: 397–415

Cannon B, Nedergaard J. Brown adipose tissue: function and physiological significance. Physiological reviews 2004; 84: 277–359

Carey AL, Formosa MF, van Every B, Bertovic D, Eikelis N, Lambert GW, Kalff V, Duffy SJ, Cherk MH, Kingwell BA. Ephedrine activates brown adipose tissue in lean but not obese humans. Diabetologia 2013; 56: 147–155

Carmeliet P, Jain RK. Molecular mechanisms and clinical applications of angiogenesis. Nature 2011; 473: 298–307

Chondronikola M, Volpi E, Børsheim E, Porter C, Annamalai P, Enerbäck S, Lidell ME, Saraf MK, Labbe SM, Hurren NM, Yfanti C, Chao T, Andersen CR, Cesani F, Hawkins H, Sidossis LS. Brown adipose tissue improves whole-body glucose homeostasis and insulin sensitivity in humans. Diabetes 2014; 63: 4089–4099

Cinti S. Anatomy of the adipose organ. Eating and weight disorders : EWD 2000; 5: 132–142

Cinti S. Adipose Organ Development and Remodeling. Comprehensive Physiology 2018; 8: 1357–1431

Clapham DE, Neer EJ. G protein beta gamma subunits. Annual review of pharmacology and toxicology 1997; 37: 167–203

Collins S, Daniel KW, Petro AE, Surwit RS. Strain-Specific Response toβ 3 -Adrenergic Receptor Agonist Treatment of Diet-Induced Obesity in Mice 1. Endocrinology 1997; 138: 405–413

Cooper DM, Mons N, Karpen JW. Adenylyl cyclases and the interaction between calcium and cAMP signalling. Nature 1995; 374: 421–424

Cypess AM. Reassessing Human Adipose Tissue. The New England journal of medicine 2022; 386: 768–779

Cypess AM, Chen Y-C, Sze C, Wang K, English J, Chan O, Holman AR, Tal I, Palmer MR, Kolodny GM, Kahn CR. Cold but not sympathomimetics activates human brown adipose tissue in vivo. Proceedings of the National Academy of Sciences of the United States of America 2012; 109: 10001–10005

Cypess AM, Lehman S, Williams G, Tal I, Rodman D, Goldfine AB, Kuo FC, Palmer EL, Tseng Y-H, Doria A, Kolodny GM, Kahn CR. Identification and importance of brown adipose tissue in adult humans. The New England journal of medicine 2009; 360: 1509–1517

Cypess AM, Weiner LS, Roberts-Toler C, Franquet Elía E, Kessler SH, Kahn PA, English J, Chatman K, Trauger SA, Doria A, Kolodny GM. Activation of human brown adipose tissue by a β3-adrenergic receptor agonist. Cell metabolism 2015; 21: 33–38

Deutsche Adipositas-Gesellschaft (DAG) e.V., Deutsche Diabetes Gesellschaf, Deutsche Gesellschaft für Ernährung e.V., Deutsche Gesellschaft für Ernährungsmedizin e.V… Interdisziplinäre Leitlinie der Qualität S3 zur „Prävention und Therapie der Adipositas“. Aktuelle Ernährungsmedizin 2014; 47

FDA. 2009. Drug Approval Package: Mozobil (plerixa) Injection NDA 22311. https://www.accessdata.fda.gov/drugsatfda_docs/nda/2008/022311s000TOC.cfm. Access date: 14/10/2022

Feng Y, Broder CC, Kennedy PE, Berger EA. HIV-1 entry cofactor: functional cDNA cloning of a seven-transmembrane, G protein-coupled receptor. Science (New York, N.Y.) 1996; 272: 872–877

Finucane MM, Stevens GA, Cowan MJ, Danaei G, Lin JK, Paciorek CJ, Singh GM, Gutierrez HR, Lu Y, Bahalim AN, Farzadfar F, Riley LM, Ezzati M. National, regional, and global trends in body-mass index since 1980: systematic analysis of health examination surveys and epidemiological studies with 960 country-years and 9·1 million participants. The Lancet 2011; 377: 557–567

Fong G-H. Mechanisms of adaptive angiogenesis to tissue hypoxia. Angiogenesis 2008; 11: 121–140

Foster DO, Frydman ML. Brown adipose tissue: the dominant site of nonshivering thermogenesis in the rat. Experientia. Supplementum 1978; 32: 147–151

Gerrits H, van Ingen Schenau DS, Bakker NEC, van Disseldorp AJM, Strik A, Hermens LS, Koenen TB, Krajnc-Franken MAM, Gossen JA. Early postnatal lethality and cardiovascular defects in CXCR7-deficient mice. Genesis (New York, N.Y. : 2000) 2008; 46: 235–245

Gesta S, Tseng Y-H, Kahn CR. Developmental origin of fat: tracking obesity to its source. Cell 2007; 131: 242–256

Hall KD, Sacks G, Chandramohan D, Chow CC, Wang YC, Gortmaker SL, Swinburn BA. Quantification of the effect of energy imbalance on bodyweight. Lancet (London, England) 2011; 378: 826–837

Hanlon CD, Andrew DJ. Outside-in signaling--a brief review of GPCR signaling with a focus on the Drosophila GPCR family. Journal of cell science 2015; 128: 3533–3542

Hanssen MJW, Hoeks J, Brans B, van der Lans AAJJ, Schaart G, van den Driessche JJ, Jörgensen JA, Boekschoten MV, Hesselink MKC, Havekes B, Kersten S, Mottaghy FM, van Marken Lichtenbelt WD, Schrauwen P. Short-term cold acclimation improves insulin sensitivity in patients with type 2 diabetes mellitus. Nat Med 2015; 21: 863–865

Heaton JM. The distribution of brown adipose tissue in the human. Journal of Anatomy 1972; 112: 35–39

Herbel JN. 2023. Mirabegron. https://www.gelbe-liste.de/wirkstoffe/Mirabegron_52349#Nebenwirkungen. Access date: 18/04/2023

Hilger D, Masureel M, Kobilka BK. Structure and dynamics of GPCR signaling complexes. Nat Struct Mol Biol 2018; 25: 4–12

Himms-Hagen J, Melnyk A, Zingaretti MC, Ceresi E, Barbatelli G, Cinti S. Multilocular fat cells in WAT of CL-316243-treated rats derive directly from white adipocytes. American journal of physiology. Cell physiology 2000; 279: C670-81

Hotamisligil GS. Inflammation and metabolic disorders. Nature 2006; 444: 860–867

Hotamisligil GS, Arner P, Caro JF, Atkinson RL, Spiegelman BM. Increased adipose tissue expression of tumor necrosis factor-alpha in human obesity and insulin resistance. The Journal of Clinical Investigation 1995; 95: 2409–2415

Janssens R, Struyf S, Proost P. The unique structural and functional features of CXCL12. Cell Mol Immunol 2018; 15: 299–311

Jing X, Yang F, Shao C, Wei K, Xie M, Shen H, Shu Y. Role of hypoxia in cancer therapy by regulating the tumor microenvironment. Molecular cancer 2019; 18: 157

Kassir R, Debs T, Blanc P, Gugenheim J, Ben Amor I, Boutet C, Tiffet O. Complications of bariatric surgery: Presentation and emergency management. International journal of surgery (London, England) 2016; 27: 77–81

Kawai T, Malech HL. WHIM syndrome: congenital immune deficiency disease. Current opinion in hematology 2009; 16: 20–26

Kershaw EE, Flier JS. Adipose tissue as an endocrine organ. The Journal of clinical endocrinology and metabolism 2004; 89: 2548–2556

Kim D, Kim J, Yoon JH, Ghim J, Yea K, Song P, Park S, Lee A, Hong C-P, Jang MS, Kwon Y, Park S, Jang MH, Berggren P-O, Suh P-G, Ryu SH. CXCL12 secreted from adipose tissue recruits macrophages and induces insulin resistance in mice. Diabetologia 2014; 57: 1456–1465

Kojima K, McQueen T, Chen Y, Jacamo R, Konopleva M, Shinojima N, Shpall E, Huang X, Andreeff M. p53 activation of mesenchymal stromal cells partially abrogates microenvironment-mediated resistance to FLT3 inhibition in AML through HIF-1α-mediated down-regulation of CXCL12. Blood 2011; 118: 4431–4439

Kretschmer C. 2016. Markteinführung von Liraglutid bei Adipositas. https://www.gelbe-liste.de/nachrichten/markteinfuehrung-liraglutid-adipositas. Access Date: 18/04/2023

Kryczek I, Lange A, Mottram P, Alvarez X, Cheng P, Hogan M, Moons L, Wei S, Zou L, Machelon V, Emilie D, Terrassa M, Lackner A, Curiel TJ, Carmeliet P, Zou W. CXCL12 and vascular endothelial growth factor synergistically induce neoangiogenesis in human ovarian cancers. Cancer Res 2005; 65: 465–472

Kurita K, Ishikawa K, Takeda K, Fujimoto M, Ono H, Kumagai J, Inoue H, Yokoh H, Yokote K. CXCL12-CXCR4 pathway activates brown adipocytes and induces insulin resistance in CXCR4-deficient mice under high-fat diet. Scientific reports 2019; 9: 6165

Lafontan M. Fat cells: afferent and efferent messages define new approaches to treat obesity. Annual review of pharmacology and toxicology 2005; 45: 119–146

Lardy HA, Ferguson SM. Oxidative phosphorylation in mitochondria. Annu. Rev. Biochem. 1969; 38: 991–1034

Liles WC, Rodger E, Broxmeyer HE, Dehner C, Badel K, Calandra G, Christensen J, Wood B, Price TH, Dale DC. Augmented mobilization and collection of CD34+ hematopoietic cells from normal human volunteers stimulated with granulocyte-colony-stimulating factor by single-dose administration of AMD3100, a CXCR4 antagonist. Transfusion 2005; 45: 295–300

Lin Z, Song J, Gao Y, Huang S, Dou R, Zhong P, Huang G, Han L, Zheng J, Zhang X, Wang S, Xiong B. Hypoxia-induced HIF-1α/lncRNA-PMAN inhibits ferroptosis by promoting the cytoplasmic translocation of ELAVL1 in peritoneal dissemination from gastric cancer. Redox biology 2022; 52: 102312

Lindberg O, Pierre J de, Rylander E, Afzelius BA. Studies of the mitochondrial energy-transfer system of brown adipose tissue. The Journal of cell biology 1967; 34: 293–310

Liu X, Wang S, You Y, Meng M, Zheng Z, Dong M, Lin J, Zhao Q, Zhang C, Yuan X, Hu T, Liu L, Huang Y, Zhang L, Wang D, Zhan J, Jong Lee H, Speakman JR, Jin W. Brown

Adipose Tissue Transplantation Reverses Obesity in Ob/Ob Mice. Endocrinology 2015; 156: 2461–2469

Loetscher M, Geiser T, O'Reilly T, Zwahlen R, Baggiolini M, Moser B. Cloning of a human seven-transmembrane domain receptor, LESTR, that is highly expressed in leukocytes. The Journal of biological chemistry 1994; 269: 232–237

Ma Q, Jones D, Borghesani PR, Segal RA, Nagasawa T, Kishimoto T, Bronson RT, Springer TA. Impaired B-lymphopoiesis, myelopoiesis, and derailed cerebellar neuron migration in CXCR4- and SDF-1-deficient mice. Proceedings of the National Academy of Sciences of the United States of America 1998; 95: 9448–9453

Maghazachi AA. Role of the heterotrimeric G proteins in stromal-derived factor-1alpha-induced natural killer cell chemotaxis and calcium mobilization. Biochemical and biophysical research communications 1997; 236: 270–274

Mau T, Yung R. Adipose tissue inflammation in aging. Experimental gerontology 2018; 105: 27–31

Meier R, Mühlethaler-Mottet A, Flahaut M, Coulon A, Fusco C, Louache F, Auderset K, Bourloud KB, Daudigeos E, Ruegg C, Vassal G, Gross N, Joseph J-M. The chemokine receptor CXCR4 strongly promotes neuroblastoma primary tumour and metastatic growth, but not invasion. PloS one 2007; 2: e1016

Mirshahi F, Pourtau J, Li H, Muraine M, Trochon V, Legrand E, Vannier J-P, Soria J, Vasse M, Soria C. SDF-1 Activity on Microvascular Endothelial Cells. Thrombosis Research 2000; 99: 587–594

Moser B, Wolf M, Walz A, Loetscher P. Chemokines: multiple levels of leukocyte migration control. Trends in immunology 2004; 25: 75–84

Nagasawa T, Hirota S, Tachibana K, Takakura N, Nishikawa S, Kitamura Y, Yoshida N, Kikutani H, Kishimoto T. Defects of B-cell lymphopoiesis and bone-marrow myelopoiesis in mice lacking the CXC chemokine PBSF/SDF-1. Nature 1996; 382: 635–638

Nagasawa T, Kikutani H, Kishimoto T. Molecular cloning and structure of a pre-B-cell growth-stimulating factor. Proceedings of the National Academy of Sciences of the United States of America 1994; 91: 2305–2309

Naumann U, Cameroni E, Pruenster M, Mahabaleshwar H, Raz E, Zerwes H-G, Rot A, Thelen M. CXCR7 functions as a scavenger for CXCL12 and CXCL11. PloS one 2010; 5: e9175

Nedergaard J, Bengtsson T, Cannon B. Unexpected evidence for active brown adipose tissue in adult humans. American journal of physiology. Endocrinology and metabolism 2007; 293: E444-452

Ni Mhurchu C, Rodgers A, Pan WH, Gu DF, Woodward M. Body mass index and cardiovascular disease in the Asia-Pacific Region: an overview of 33 cohorts involving 310 000 participants. International journal of epidemiology 2004; 33: 751–758

Nicholls DG, Bernson VS, Heaton GM. The identification of the component in the inner membrane of brown adipose tissue mitochondria responsible for regulating energy dissipation. Experientia. Supplementum 1978; 32: 89–93

Nnodim JO, Lever JD. Neural and vascular provisions of rat interscapular brown adipose tissue. The American journal of anatomy 1988; 182: 283–293

Oberlin E, Amara A, Bachelerie F, Bessia C, Virelizier JL, Arenzana-Seisdedos F, Schwartz O, Heard JM, Clark-Lewis I, Legler DF, Loetscher M, Baggiolini M, Moser B. The CXC chemokine SDF-1 is the ligand for LESTR/fusin and prevents infection by T-cell-line-adapted HIV-1. Nature 1996; 382: 833–835

Obradovic M, Sudar-Milovanovic E, Soskic S, Essack M, Arya S, Stewart AJ, Gojobori T, Isenovic ER. Leptin and Obesity: Role and Clinical Implication. Frontiers in endocrinology 2021; 12: 585887

Odemis V, Lipfert J, Kraft R, Hajek P, Abraham G, Hattermann K, Mentlein R, Engele J. The presumed atypical chemokine receptor CXCR7 signals through G(i/o) proteins in primary rodent astrocytes and human glioma cells. Glia 2012; 60: 372–381

Padwal R, Li SK, Lau DCW. Long-term pharmacotherapy for obesity and overweight. The Cochrane database of systematic reviews 2003: CD004094

Peng H, Zhang H, Zhu H. Blocking CXCR7-mediated adipose tissue macrophages chemotaxis attenuates insulin resistance and inflammation in obesity. Biochemical and biophysical research communications 2016; 479: 649–655

Pfeifer A, Hoffmann LS. Brown, beige, and white: the new color code of fat and its pharmacological implications. Annual review of pharmacology and toxicology 2015; 55: 207–227

Prospective Studies Collaboration. Body-mass index and cause-specific mortality in 900 000 adults: collaborative analyses of 57 prospective studies. Lancet (London, England) 2009; 373: 1083–1096

Puigserver P, Wu Z, Park CW, Graves R, Wright M, Spiegelman BM. A Cold-Inducible Coactivator of Nuclear Receptors Linked to Adaptive Thermogenesis. Cell 1998; 92: 829–839

Rajagopal S, Kim J, Ahn S, Craig S, Lam CM, Gerard NP, Gerard C, Lefkowitz RJ. Beta-arrestin- but not G protein-mediated signaling by the "decoy" receptor CXCR7. Proceedings of the National Academy of Sciences of the United States of America 2010; 107: 628–632

Roberto CA, Swinburn B, Hawkes C, Huang TT-K, Costa SA, Ashe M, Zwicker L, Cawley JH, Brownell KD. Patchy progress on obesity prevention: emerging examples, entrenched barriers, and new thinking. The Lancet 2015; 385: 2400–2409

Rosen ED, MacDougald OA. Adipocyte differentiation from the inside out. Nat Rev Mol Cell Biol 2006; 7: 885–896

Rosen ED, Spiegelman BM. What we talk about when we talk about fat. Cell 2014; 156: 20–44

Rubin JB. Chemokine signaling in cancer: one hump or two? Seminars in cancer biology 2009; 19: 116–122

Sadri F, Rezaei Z, Fereidouni M. The significance of the SDF-1/CXCR4 signaling pathway in the normal development. Molecular biology reports 2022; 49: 3307–3320

Saghizadeh M, Ong JM, Garvey WT, Henry RR, Kern PA. The expression of TNF alpha by human muscle. Relationship to insulin resistance. The Journal of Clinical Investigation 1996; 97: 1111–1116

Sassone-Corsi P. The cyclic AMP pathway. Cold Spring Harbor perspectives in biology 2012; 4

Schioppa T, Uranchimeg B, Saccani A, Biswas SK, Doni A, Rapisarda A, Bernasconi S, Saccani S, Nebuloni M, Vago L, Mantovani A, Melillo G, Sica A. Regulation of the chemokine receptor CXCR4 by hypoxia. The Journal of experimental medicine 2003; 198: 1391–1402

Schneider CA, Rasband WS, Eliceiri KW. NIH Image to ImageJ: 25 years of image analysis. Nature methods 2012; 9: 671–675

Seale P, Bjork B, Yang W, Kajimura S, Chin S, Kuang S, Scimè A, Devarakonda S, Conroe HM, Erdjument-Bromage H, Tempst P, Rudnicki MA, Beier DR, Spiegelman BM. PRDM16 controls a brown fat/skeletal muscle switch. Nature 2008; 454: 961–967

Seale P, Kajimura S, Yang W, Chin S, Rohas LM, Uldry M, Tavernier G, Langin D, Spiegelman BM. Transcriptional control of brown fat determination by PRDM16. Cell metabolism 2007; 6: 38–54

Serhan CN, Chiang N, van Dyke TE. Resolving inflammation: dual anti-inflammatory and pro-resolution lipid mediators. Nature reviews. Immunology 2008; 8: 349–361

Shirozu M, Nakano T, Inazawa J, Tashiro K, Tada H, Shinohara T, Honjo T. Structure and chromosomal localization of the human stromal cell-derived factor 1 (SDF1) gene. Genomics 1995; 28: 495–500

Simon GE, Korff M von, Saunders K, Miglioretti DL, Crane PK, van Belle G, Kessler RC. Association between obesity and psychiatric disorders in the US adult population. Archives of general psychiatry 2006; 63: 824–830

Smathers RL, Petersen DR. The human fatty acid-binding protein family: evolutionary divergences and functions. Human genomics 2011; 5: 170–191

Stanisavljević L, Aßmus J, Storli KE, Leh SM, Dahl O, Myklebust MP. CXCR4, CXCL12 and the relative CXCL12-CXCR4 expression as prognostic factors in colon cancer. Tumour biology : the journal of the International Society for Oncodevelopmental Biology and Medicine 2016; 37: 7441–7452

Stork PJ, Schmitt JM. Crosstalk between cAMP and MAP kinase signaling in the regulation of cell proliferation. Trends in Cell Biology 2002; 12: 258–266

Sun Y, Cheng Z, Ma L, Pei G. Beta-arrestin2 is critically involved in CXCR4-mediated chemotaxis, and this is mediated by its enhancement of p38 MAPK activation. The Journal of biological chemistry 2002; 277: 49212–49219

Sun Y, Xiong X, Wang X. RELA promotes hypoxia-induced angiogenesis in human umbilical vascular endothelial cells via LINC01693/miR-302d/CXCL12 axis. Journal of cellular biochemistry 2019; 120: 12549–12558

Tabatabai G, Frank B, Möhle R, Weller M, Wick W. Irradiation and hypoxia promote homing of haematopoietic progenitor cells towards gliomas by TGF-beta-dependent HIF-1alpha-mediated induction of CXCL12. Brain 2006; 129: 2426–2435

Tan W, Martin D, Gutkind JS. The Galpha13-Rho signaling axis is required for SDF-1-induced migration through CXCR4. The Journal of biological chemistry 2006; 281: 39542–39549

Tanaka T, Yoshida N, Kishimoto T, Akira S. Defective adipocyte differentiation in mice lacking the C/EBPbeta and/or C/EBPdelta gene. The EMBO Journal 1997; 16: 7432–7443

Timmons JA, Wennmalm K, Larsson O, Walden TB, Lassmann T, Petrovic N, Hamilton DL, Gimeno RE, Wahlestedt C, Baar K, Nedergaard J, Cannon B. Myogenic gene expression signature establishes that brown and white adipocytes originate from distinct cell lineages. Proceedings of the National Academy of Sciences of the United States of America 2007; 104: 4401–4406

Tseng Y-H, Kokkotou E, Schulz TJ, Huang TL, Winnay JN, Taniguchi CM, Tran TT, Suzuki R, Espinoza DO, Yamamoto Y, Ahrens MJ, Dudley AT, Norris AW, Kulkarni RN, Kahn CR. New role of bone morphogenetic protein 7 in brown adipogenesis and energy expenditure. Nature 2008; 454: 1000–1004

Tu TC, Nagano M, Yamashita T, Hamada H, Ohneda K, Kimura K, Ohneda O. A Chemokine Receptor, CXCR4, Which Is Regulated by Hypoxia-Inducible Factor 2α, Is Crucial for Functional Endothelial Progenitor Cells Migration to Ischemic Tissue and Wound Repair. Stem cells and development 2016; 25: 266–276

Uchida T, Rossignol F, Matthay MA, Mounier R, Couette S, Clottes E, Clerici C. Prolonged hypoxia differentially regulates hypoxia-inducible factor (HIF)-1alpha and HIF-2alpha expression in lung epithelial cells: implication of natural antisense HIF-1alpha. The Journal of biological chemistry 2004; 279: 14871–14878

van den Berg SM, van Dam AD, Rensen PCN, Winther MPJ de, Lutgens E. Immune Modulation of Brown(ing) Adipose Tissue in Obesity. Endocrine reviews 2017; 38: 46–68

van Marken Lichtenbelt WD, Schrauwen P, van de Kerckhove S, Westerterp-Plantenga MS. Individual variation in body temperature and energy expenditure in response to mild cold. American journal of physiology. Endocrinology and metabolism 2002; 282: E1077-1083

Vandyke K, Zeissig MN, Hewett DR, Martin SK, Mrozik KM, Cheong CM, Diamond P, To LB, Gronthos S, Peet DJ, Croucher PI, Zannettino ACW. HIF-2α Promotes Dissemination of Plasma Cells in Multiple Myeloma by Regulating CXCL12/CXCR4 and CCR1. Cancer Res 2017; 77: 5452–5463

Vila-Coro AJ, Rodríguez-Frade JM, Martín De Ana A, Moreno-Ortíz MC, Martínez-A C, Mellado M. The chemokine SDF-1alpha triggers CXCR4 receptor dimerization and activates the JAK/STAT pathway. FASEB journal : official publication of the Federation of American Societies for Experimental Biology 1999; 13: 1699–1710

Virtanen KA, Lidell ME, Orava J, Heglind M, Westergren R, Niemi T, Taittonen M, Laine J, Savisto N-J, Enerbäck S, Nuutila P. Functional brown adipose tissue in healthy adults. The New England journal of medicine 2009; 360: 1518–1525

Vosselman MJ, van der Lans AAJJ, Brans B, Wierts R, van Baak MA, Schrauwen P, van Marken Lichtenbelt WD. Systemic β-adrenergic stimulation of thermogenesis is not accompanied by brown adipose tissue activity in humans. Diabetes 2012; 61: 3106–3113

Westerberg R, Månsson J-E, Golozoubova V, Shabalina IG, Backlund EC, Tvrdik P, Retterstøl K, Capecchi MR, Jacobsson A. ELOVL3 is an important component for early onset of lipid recruitment in brown adipose tissue. The Journal of biological chemistry 2006; 281: 4958–4968

Wettschureck N, Offermanns S. Mammalian G proteins and their cell type specific functions. Physiological reviews 2005; 85: 1159–1204

WHO. 2021a. Cardiovascular diseases. https://www.who.int/news-room/fact-sheets/detail/cardiovascular-diseases-(cvds). Access date: 11/08/2022.

WHO. 2021b. Diabetes. https://www.who.int/news-room/fact-sheets/detail/diabetes. Access date: 11/08/2022

WHO. 2021c Obesity and overweight. https://www.who.int/news-room/fact-sheets/detail/obesity-and-overweight. Access date: 11/08/2022

Wu B, Wang L, Yang X, Mao M, Ye C, Liu P, Yang Z, Yang X, Lei D, Zhang C. Norepinephrine inhibits mesenchymal stem cell chemotaxis migration by increasing stromal cell-derived factor-1 secretion by vascular endothelial cells via NE/abrd3/JNK pathway. Experimental cell research 2016; 349: 214–220

Wu J, Boström P, Sparks LM, Ye L, Choi JH, Giang A-H, Khandekar M, Virtanen KA, Nuutila P, Schaart G, Huang K, Tu H, van Marken Lichtenbelt WD, Hoeks J, Enerbäck S, Schrauwen P, Spiegelman BM. Beige adipocytes are a distinct type of thermogenic fat cell in mouse and human. Cell 2012; 150: 366–376

Wu J, Cohen P, Spiegelman BM. Adaptive thermogenesis in adipocytes: is beige the new brown? Genes & development 2013; 27: 234–250

Yao L, Heuser-Baker J, Herlea-Pana O, Zhang N, Szweda LI, Griffin TM, Barlic-Dicen J. Deficiency in adipocyte chemokine receptor CXCR4 exacerbates obesity and compromises thermoregulatory responses of brown adipose tissue in a mouse model of diet-induced obesity. FASEB journal : official publication of the Federation of American Societies for Experimental Biology 2014; 28: 4534–4550

Yee Koh M, Spivak-Kroizman TR, Powis G. HIF-1 regulation: not so easy come, easy go. Trends in biochemical sciences 2008; 33: 526–534

Yoneshiro T, Aita S, Matsushita M, Kayahara T, Kameya T, Kawai Y, Iwanaga T, Saito M. Recruited brown adipose tissue as an antiobesity agent in humans. The Journal of Clinical Investigation 2013; 123: 3404–3408

Yoshida T, Sakane N, Wakabayashi Y, Umekawa T, Kondo M. Anti-obesity and anti-diabetic effects of CL 316, 243, a highly specific β3-adrenoceptor agonist, in yellow KK mice. Life Sciences 1994; 54: 491–498

Yu L, Cecil J, Peng S-B, Schrementi J, Kovacevic S, Paul D, Su EW, Wang J. Identification and expression of novel isoforms of human stromal cell-derived factor 1. Gene 2006; 374: 174–179

Yu X, Wang D, Wang X, Sun S, Zhang Y, Wang S, Miao R, Xu X, Qu X. CXCL12/CXCR4 promotes inflammation-driven colorectal cancer progression through activation of RhoA signaling by sponging miR-133a-3p. Journal of experimental & clinical cancer research : CR 2019; 38: 32

Zhang M, Qiu L, Zhang Y, Xu D, Zheng JC, Jiang L. CXCL12 enhances angiogenesis through CXCR7 activation in human umbilical vein endothelial cells. Sci Rep 2017; 7: 8289

Zhang Y, Proenca R, Maffei M, Barone M, Leopold L, Friedman JM. Positional cloning of the mouse obese gene and its human homologue. Nature 1994; 372: 425–432

Ziegler ME, Hatch MMS, Wu N, Muawad SA, Hughes CCW. mTORC2 mediates CXCL12-induced angiogenesis. Angiogenesis 2016; 19: 359–371

Zlotnik A, Yoshie O. Chemokines: a new classification system and their role in immunity. Immunity 2000; 12: 121–127

9. Acknowledgements

First of all, I would like to thank Prof. Alexander Pfeifer for the opportunity to perform research for my thesis at the institute of pharmacology and toxicology. Further, I would like to thank him and Dr. Staffan Hildebrand for supervising my work, interpreting data in a critical fashion and finally for all the scientifc freedom I had during my studies. I truly learned a lot during my time at the IPT.

Moreover, I am very thankful for all the support from other members of the IPT. Especially, I would like to thank Caro, Laura, Daniel, Birte, Dennis, Martin, and Babsi for all of the fun times, as well as all of the scientific advise! Further, a special thanks goes out to Markus Raspe, who was always there and ready to help when I had difficulties with technical things in the lab.

Also, I want to thank my family and friends for the constant support and - literally - always being there. Thanks to my roommate Simon for all the great academic discussions in our kitchen. Thanks, Anton, for all the creativity-enhancing talks. Another special thanks goes out to Franzi for your great advise on illustrations and to Lina for your help and feedback while writing the thesis!

Furthermore, I want to thank my mother, Katja, my stepfather, Oleg, my sister, Luka, my grandparents, Inga and Malte, and my uncle, Andrej. Words cannot describe how grateful I am for the amount of support I have constantly received.

At last, another very special thanks goes out to my partner, Jasmin. Thanks for proofreading, motivating me, and helping me whenever I needed help. I am incredibly grateful for your loving and caring nature. You are literally always there and I know that I can always rely on you!